Coordination Chemistry Reviews 254 (2010) 972–990

Contents lists available at ScienceDirect

Coordination Chemistry Reviews

journal homepage: www.elsevier.com/locate/ccr

Review

Recent advances in the sensitized luminescence of organic europium complexes

Yan Ma, Yuan Wang*

Beijing National Laboratory for Molecular Sciences, State Key Laboratory for Structural Chemistry of Unstable and Stable Species, College of Chemistry & Molecular Engineering, Peking University, Beijing 100871, PR China

Contents

ARTICLE INFO

Article history:
Received 29 November 2009
Accepted 10 February 2010
Available online 18 February 2010

Keywords:
Lanthanide complex
Energy-transfer mechanisms
Long-wavelength sensitization
Nanoparticle
Bioimaging
Two-photon-excitation

ABSTRACT

In this paper, recent advances in the synthesis, mechanism of sensitized emission, and luminescent properties of organic lanthanide complexes are reviewed. Stress is put on the progress in the development of organic europium complexes and their nanoparticles with excellent visible-light-sensitized and two-photon-sensitized Eu^{III} luminescence properties. These are of increasing importance because bioanalysis or bioimaging techniques based on such labeled materials will combine the advantages of high sensitivity, high signal-to-noise ratio, deep penetration, and low photodamage to biological samples. In addition, the application of long-wavelength-sensitized luminescence of organic lanthanide complexes and their nanoparticles in bioimaging is discussed.

1. Introduction

The emission of trivalent lanthanide (Ln^{III}) ions covers the spectroscopic range (0.3–3 μm) from ultraviolet to visible and near-infrared (NIR) light (e.g., ultraviolet, blue, green, orange and red light of Gd^{III}, Tm^{III}, Tb^{III}, Sm^{III}, and Eu^{III} ion, respectively, and NIR light of Nd^{III}, Ho^{III}, Er^{III}, and Yb^{III} ion) [1,2]. Ln^{III} ions have the $[Xe]4f^n$ (n = 0–14) electronic configurations. The 4*f* orbitals of Ln^{III} ions are shielded by the filled $5s^25p^6$ sub-shells, which endows Ln^{III} ions with narrow-line emission bands. The 4*f*–4*f* electronic transitions in Ln^{III} ions are forbidden by the electric dipole selection rules because the parity of the initial electronic states is the same with that of the final states. However, the selection rules are relaxed by several mechanisms. An important one is the temporary changes of the geometric arrangement around the Ln^{III} ions by the molecular vibration. Other mechanisms which cause a breakdown of the selection rules are *J*-mixing and the mixing with opposite-parity wavefunctions, such as 5*d* orbitals, ligand orbitals or charge transfer states [3]. The low probability of the electric dipole *f*–*f* transitions

Abbreviations: MK, Michler's ketone (4,4′-bis(*N*,*N*-dimethylamino)benzophenone); fod, 6,6,7,7,8,8,8-hepta-fluoro-2,2-dimethyloctane-3,4-dione; HPHN, 9-hydroxyphenal-1-one; H_4tsdb, *N*,*N*′,*N*″,*N*‴-tetrasalicylidene-3,3′-diaminobenzidine; dpbt, 2-(*N*,*N*-diethylanilin-4-yl)-4,6-bis(3,5-dimethyl-pyrazol-1-yl)-1,3,5-triazine; tta, thenoyltrifluoroacetonato; dmbpt, 2-(*N*,*N*-diethyl-2,6-dimethylanilin-4-yl)-4,6-bis(3,5-dimethylpyrazol-1-yl)-1,3,5-triazene; dda, *N*,*N*-diethyl-2,6-dimethylanilin; dmt, 2-(*N*,*N*-diethyl-2,6-dimethylanilin-4-yl)-4,6-dichloro-1,3,5-triazine; nendta, *N*-ethyl-*N*-(4,6-dichloro-1,3,5-triazine-2-yl)-2,6-dimethyl-anilin; PTBS, poly(4-tert-butyl styrene); bpt, 2-(*N*,*N*-diethylanilin-4-yl)-4,6-bis(pyrazol-1-yl)-1,3,5-triazine; DEASPI, *trans*-4-[*p*-(*N*,*N*-diethyl-amino) styryl]-*N*-methylpyridinium; nta, naphthoyltrifluoroacetone; DPA, pyridine dicarboxylic acid; HG, 3,4,5-tris(triethylene-glycol)phenyl; DCM, 4-dicyano-methylene-2-methyl-6-*p*-dimethylaminostyryl-4H-pyran; CDHH, 5-(4″-chloro-sulfo-1′,1″-diphenyl-4′-yl)-1,1,1,2,2,3,3-heptafluoro-4,6-hexanedione; APS, 3-aminopropyl(triethoxyl)silane; TEOS, tetraethyl orthosilicate; BHHCT, 4,4′-bis(1″,1″,1″,2″,2″,3″,3″-heptafluoro-4″,6″-hexanedion-6″-yl)chloro-sulfo-o-terphenyl.

* Corresponding author.
E-mail address: wangy@pku.edu.cn (Y. Wang).

0010-8545/$ – see front matter © 2010 Elsevier B.V. All rights reserved.
doi:10.1016/j.ccr.2010.02.013

on the one hand gives rise to the long lifetimes of the Ln^{III} luminescence, but on the other hand causes the very low molar extinction coefficients (typically 1–10 M^{-1} cm^{-1}) of Ln^{III} ions, which makes it difficult to directly excite the Ln^{III} ions by light. To overcome this problem, organic antenna chromophores are usually used to sensitize Ln^{III} ions via energy transfer from the chromophores to Ln^{III} ions. The magnetic dipole and the electric quadrupole *f–f* transitions of Ln^{III} ions have been reviewed by Bünzli and Eliseeva [3b,c].

The sensitization of lanthanide ions usually proceeds in three steps. First, light is absorbed by the organic antenna chromophores coordinated or close to the lanthanide ions. Energy is then transferred to one or several excited-states of the metal ions, and finally, the metal ions emit light via the radiative deactivation of the luminescent states. This sensitization process is much more effective than the direct excitation of Ln^{III} ions. The overall luminescence quantum yield (Φ^{L}_{Ln}) of the centered ions in the complexes can be expressed as follows:

$$\Phi^{L}_{Ln} = \eta_{sens}\Phi^{Ln}_{Ln} \quad (1)$$

where Φ^{L}_{Ln} and Φ^{Ln}_{Ln} are the quantum yields resulting from indirect and direct excitation, respectively, and η_{sens} represents the efficiency of energy transfer from the antenna ligand to the centered ion [4–8].

Although a number of sensitized Ln^{III} complexes have been reported, energy-transfer pathways have not been fully understood for the sensitization of the lanthanide ions. To date, two energy-transfer pathways for the sensitization emission of lanthanide complexes have been proposed. The first is the often observed triplet pathway of energy transfer through the triplet excited-states (T_1) of antenna ligands; while the second starts from the singlet excited-states (S_1) of the chromophore ligands and does not involve the T_1 states of the antenna ligands, the so-called singlet energy-transfer pathway.

Energy transfer from the triplet states of antenna ligands, converting from the S_1 states via intersystem crossing (ISC), to the Ln^{III} ions occurs in many lanthanide complexes as confirmed by most of the experimental work conducted on the sensitization mechanism of luminescent lanthanide complexes [9]. Therefore, most research on the development of antenna chromophores for the sensitization of lanthanide ion luminescence was focused on the design and synthesis of antenna ligands with a T_1 state matching the energy gaps of Ln^{III} ions in order to promote the energy-transfer process. For most Eu^{III} complexes developed with this strategy, the optical excitation windows appear to be limited to less than 385 nm owing to the energetic constraints from the T_1 states of the ligands [9c,10].

For application in biosensing or bioimaging, great efforts have been focused on the development of luminescent Ln^{III} complexes capable of being efficiently sensitized by long-wavelength light, because the long-wavelength light is less harmful to biological tissue, allowing deep penetration, causing less background fluorescence and thus lessening the interferences from biological samples [11]. The NIR-emitting Ln^{III} ions, such as Nd^{III}, Yb^{III}, and Er^{III}, have been attracting considerable attention since biological tissues are fairly optically transparent in the spectroscopic range from 700 nm to 1000 nm [2]. However, until now, very few NIR-emitting Ln^{III} complexes have been used as probes in the practical applications of bioimaging and bioassay because of their low luminescence quantum yields.

Due to the characteristic luminescence properties of Eu^{III} complexes, such as the characteristic narrow-line emission in the red-light region with acceptable transparence for many biosamples, large Stokes shifts, high luminescence quantum yields, and long luminescence lifetime (millisecond order), the long-wavelength sensitization of Eu^{III} complexes is of significance for the application in life science [12–16].

Two strategies have been adopted to extend the excitation window of Eu^{III} complexes to a long-wavelength region. Diminishing the energy gap between the lowest S_1 state and the T_1 state of the antenna ligand is considered an effective way to extend the excitation wavelength for the Eu^{III} complex into the visible-light region through the usual triplet energy-transfer pathway; this has been demonstrated by several research groups [17–20]. Another promising route to realize the longer-wavelength sensitization of Eu^{III} emission is through the singlet energy-transfer pathway. In this way the energetic constraints from the T_1 state of the ligand can be avoided.

The contribution of the singlet energy-transfer pathway for the sensitization of lanthanide luminescence was thought to be very low in the past, because the rate of ISC in luminescent lanthanide complexes is very fast, and this was true for the most known lanthanide complexes [21,22]. The singlet pathway was first proposed by Kleinerman in 1966 [23]. Horrocks and co-workers later examined the energy-transfer processes in Tb^{III}-binding proteins and speculated that it was the singlet excited-state of the chromophore that sensitized the Tb^{III} emission [24,25]. However, owing to the lack of information regarding the emission from the excited-states, especially the T_1 state, of the coordinated ligand and the difficulties in the determination of the ligand-localized triplet–triplet absorption spectra for lanthanide complexes, it is very difficult to prove for certain which state is mainly responsible for the energy-transfer process in many lanthanide complexes [26,27].

The singlet energy-transfer pathway was first demonstrated by a series of credible experiments of excited-state dynamics of a novel Eu^{III} complex $Eu(tta)_3dpbt$ [28]. However, intensive efforts are necessary to confirm whether the ligand-to-metal charge transfer (LMCT) states, which were referred to in several articles concerning the energy-transfer mechanism of the lanthanide complexes [29,30], are involved in the singlet energy-transfer pathway of $Eu(tta)_3dpbt$.

This review will give an overview on the recent advances in the synthesis, sensitization mechanism, and luminescent property of organic lanthanide complexes. In this review, we do not strive to carry out an exhaustive survey of the field; instead, we seek to provide a discussion on the progress in developing europium complexes capable of being efficiently excited by visible-light or multiphoton absorption of NIR light. The preparation of desirable luminescent nanoparticles containing organic Eu^{III} complexes with long-wavelength sensitized luminescence properties and their application in life sciences is also considered.

2. Synthesis and luminescent properties of visible-light-sensitized europium complexes

2.1. Europium complexes sensitized by long-wavelength light

Eu^{III} complexes with excitation wavelengths longer than 400 nm were reported before 1999 [9d,31], but the overall luminescence quantum yields of the central ion in these systems are generally low, partly due to the back energy-transfer process from the Eu^{III} emitting level to the ligand T_1 state. For example, the complex $[NaEu(tsdb)]_n$ reported by Thompson and co-workers [9d] exhibited an absorption band centered at 408 nm and a quantum yield of Eu^{III} luminescence of 0.02.

The first example for the efficient long-wavelength sensitization of the Eu^{III} luminescence was reported by Verhoeven and co-workers in 1999 [17]. A solution of 10^{-5} M Michler's ketone (4,4′-bis(*N*,*N*-dimethylamino)benzophenone, MK) and 10^{-4} M $Eu(fod)_3$ (fod = 6,6,7,7,8,8,8-hepta-fluoro-2,2-dimethyloctane-3,4-dione) (Scheme 1) in benzene emitted the characteristic red glow of the Eu^{III} ion under daylight illumination. The excitation spec-

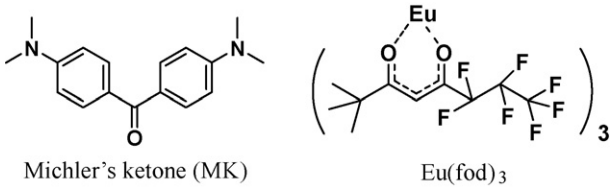

Scheme 1. Structure of Michler's ketone (MK).

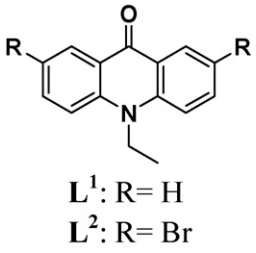

Scheme 2. Structures of acridone derivatives **L¹** and **L²**.

trum for Eu^{III} luminescence showed a wide excitation window in the visible-light region extending beyond 450 nm. Titration experimental results indicated the formation of MK-Eu(fod)$_3$ complex in benzene with a MK/Eu(fod)$_3$ ratio of 1:1. The luminescence quantum yield was found to be 0.17 in aerated solution and 0.20 after deoxygenation (upon excitation at 420 nm). It was considered that the very small singlet–triplet energy gap of MK is the crucial point for the efficient long-wavelength sensitization of the Eu^{III} luminescence.

In another study, two acridone derivatives **L¹** and **L²** (Scheme 2) with low singlet–triplet energy gaps, were found to sensitize the luminescence of Eu^{III} ion under excitation in visible-light region via the intermolecular energy-transfer processes [9e]. The mixture of Eu(fod)$_3$ and **L¹**/**L²** (with a ratio of Eu(fod)$_3$ to L^1 or L^2 of 1:1) displayed excitation bands at about 415 nm/432 nm, regardless of solvent polarity. Unfortunately, the luminescence quantum yields of these complexes were not provided. It should be mentioned that the stability of Eu^{III} complexes with a monodentate antenna ligand such as MK, **L¹** or **L²** seems not satisfying for many practical applications in solutions.

Another series of long-wavelength-sensitized Eu^{III} complexes reported by Sammes and co-workers also possess acridone chromophores as the sensitizers [9e,18]. The through space energy-transfer from acridone chromophores to Eu^{III} ion could occur when the acridone group in the complexes was not directly coordinated to Eu^{III} ion, but linked via a chain to other coordinated chelating-ligands (Scheme 3). Eu**L³** and Eu**L⁴** were stable, charge-neutral, and water soluble; however, their luminescence quantum yields were determined to be only 0.014 and 0.01, respectively, which might be attributed to the unsuitable relative position between the acridone group and Eu^{III} ion.

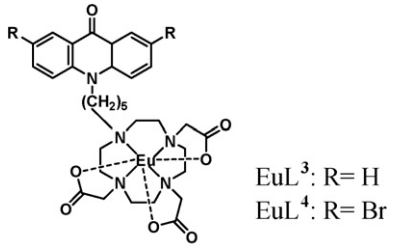

Scheme 3. Structure of complexes Eu**L³**.

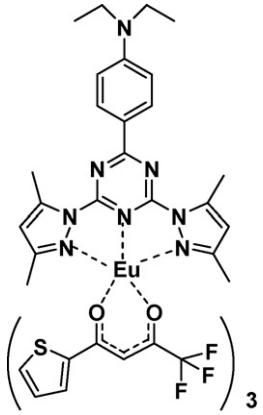

Scheme 4. Structure of complex Eu(tta)$_3$dpbt.

A Eu^{III} complex with 9-hydroxyphenal-1-one (HPHN) as an antenna ligand coordinating with Eu^{III} ion in a bidentate fashion was reported by Van Deun et al. [32]. HPHN molecule has an electron-rich three-ring structure, and an intramolecular hydrogen bonding between the 9-hydroxy proton and the 1-carbonyl oxygen atom. The ligand formed stable 3:1 complexes with Eu^{III} ion. The excitation spectrum of this complex exhibited three bands centered at 250, 350 and 458 nm, respectively. The small singlet–triplet gap of HPHN was the main reason for the visible-light-sensitized luminescence of this complex. Upon the excitation at 458 nm, the luminescence quantum yield of this complex was quite low, with the value of 0.005.

In 2004, we reported an interesting complex Eu(tta)$_3$dpbt (dpbt = 2-(*N*,*N*-diethylanilin-4-yl)-4,6-bis(3,5-dimethyl-pyrazol-1-yl)-1,3,5-triazine, tta = thenoyltrifluoroacetonato, Scheme 4) [28], which exhibits highly efficient Eu^{III} luminescence and an excitation window extending up to 440 nm in a dilute toluene solution (1×10^{-5} M). The excitation window of Eu(tta)$_3$dpbt can be extended beyond 460 nm when the concentration is increased to 1×10^{-2} M.

The overall luminescence quantum yields for the Eu^{III} emission of the complex in toluene is 0.5 as confirmed later (λ_{ex} = 402 nm, 283 K, DCM in *n*-propanol as the reference (Φ = 0.57)).

As shown in Fig. 1, the excitation spectrum of Eu(tta)$_3$dpbt (emission monitored at 614 nm) is in agreement with its ground state absorption spectrum at the long-wavelength spectroscopic

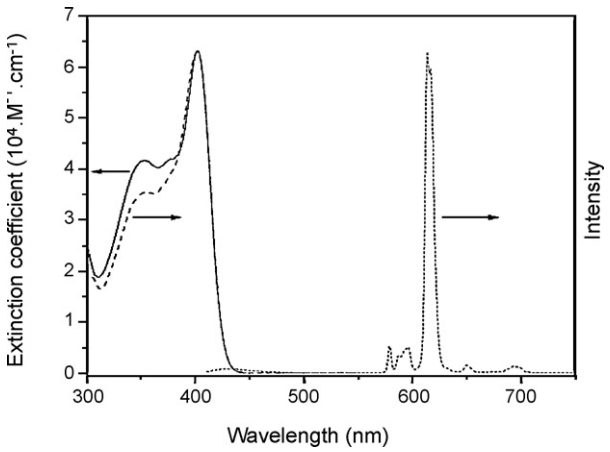

Fig. 1. Room temperature UV/vis absorption (solid line), fluorescence excitation (dashed line; λ_{em} = 614 nm), and fluorescence emission (dotted line; λ_{ex} = 402 nm) spectra of Eu(tta)$_3$dpbt in toluene (4.3×10^{-6} M). Spectra are normalized to the absorption maximum.

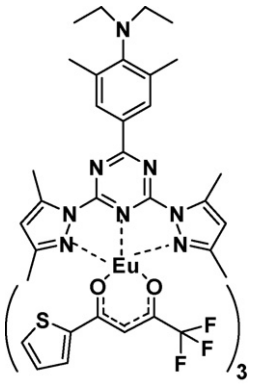

Scheme 5. Structure of complex Eu(tta)$_3$dmbpt.

region, implying the sensitization of Eu^{III} luminescence is efficient in the visible-light region.

Upon excitation with visible-light, Eu(tta)$_3$dpbt exhibits not only highly efficient Eu^{III} luminescence, but also high brightness which defines as the product of ε_{ex} (the molar extinction coefficient at the wavelength of the excitation) and Φ_F (the luminescence quantum yield of the Eu^{III} emission).

Later, we reported another Eu^{III} complex Eu(tta)$_3$dmbpt (dmbpt = 2-(*N*,*N*-diethyl-2,6-dimethylanilin-4-yl)-4,6-bis(3,5-dimethylpyrazol-1-yl)-1,3,5-triazine), Scheme 5), which exhibits a broad single-photon excitation window extending up to 458 nm even in a dilute toluene solution (1×10^{-5} M) and almost the same luminescent quantum yield as that of Eu(tta)$_3$dpbt [33].

Eu(tta)$_3$dmbpt was designed by introducing two methyl groups at the 2,6-positions of the phenyl ring in Eu(tta)$_3$dpbt. Fig. 2 shows the molecular structures of ligands dpbt and dmbpt. In dpbt, the –N(CH$_2$–)$_2$ moiety of diethylamino almost locates in the same plane with the phenyl ring. While in dmbpt the interplane twist angle between the –N(CH$_2$–)$_2$ moiety and the phenyl ring is close to 90°, which is caused by the strong steric repulsion between the diethylamino and 2,6-dimethyl groups on the phenyl ring. According to the crystallographic data, in dpbt, the hybrid orbital of N in diethylamino group is close to sp^2, with the lone electron pair of N participating in the conjugation system. While, in dmbpt, the hybrid orbital of N in diethylamino group is close to sp^3, suggesting a severe twist between the nitrogen lone-pair electrons and the aromatic system for dmbpt in the ground state.

Because of the change in the molecular structure between dpbt and dmbpt, the synthesis route for dmbpt had to be improved to obtain a reasonable yield. Owing to the twisted conjugation of the N atom, the alkalescence of the diethylamino group in *N*,*N*-diethyl-2,6-dimethylanilin (dda) is stronger than that in *N*,*N*-diethylanilin. As a result, the synthesis route that we adopted to synthesize dpbt (Scheme 6) was not efficient for the synthesis of dmbpt. Simply heating a mixture of cyanuric chloride and dda produced only a small amount of 2-(*N*,*N*-diethyl-2,6-dimethylanilin-4-yl)-4,6-dichloro-1,3,5-triazine (dmt) (less than 1%), while the dominant product was *N*-ethyl-*N*-(4,6-dichloro-1,3,5-triazine-2-yl)-2,6-dimethyl-anilin (nendta), formed via the reaction between the diethylamino group of *N*,*N*-diethyl-2,6-dimethylanilin and 2,4,6-trichloro-1,3,5-triazine. In order to synthesize Eu(tta)$_3$dmbpt efficiently, we adopted an alternative route to synthesize dmt, as shown in Scheme 7, in which dmt formed via the reaction between *N*,*N*-diethyl-2,6-dimethyl-4-phenyllithium and cyanuric chloride with a yield higher than 50%.

As shown in the UV–vis absorption spectrum of Eu(tta)$_3$dmbpt (Fig. 3), because of the severely twisted conjugation system of the antenna ligand dmbpt, the molar extinction coefficient of the

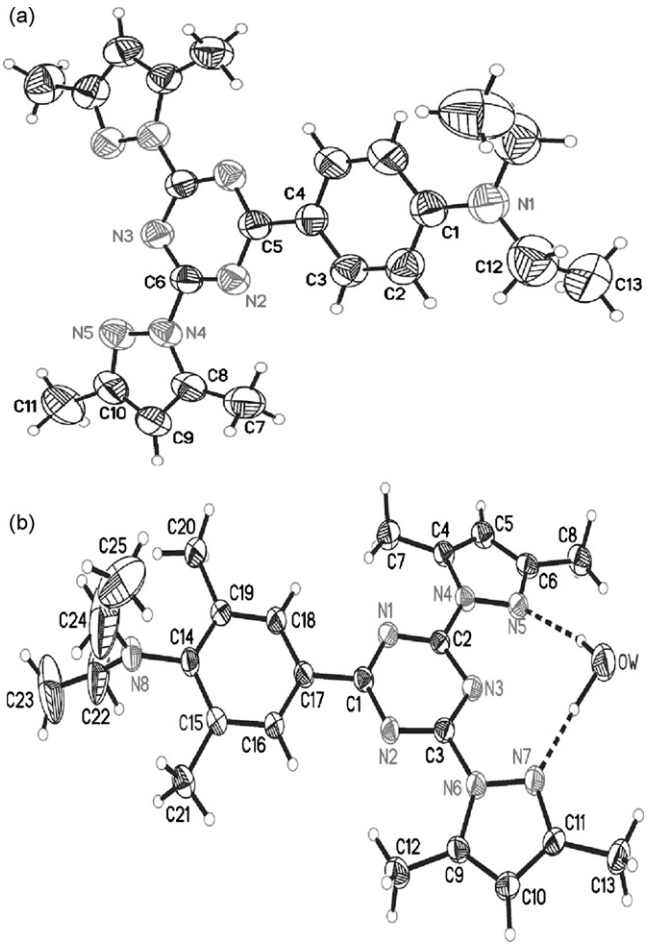

Fig. 2. Molecular structures of chromophore ligands: (a) dpbt obtained from a crystal of size 0.46 mm × 0.42 mm × 0.15 mm; (b) dmbpt·H$_2$O obtained from a crystal of size 0.60 mm × 0.18 mm × 0.10 mm. A water molecule was bonded to the two pyrazole groups by hydrogen bonding during the growth of the single crystal. Figure was reproduced from Ref. [33], with permission of the copyright holders.

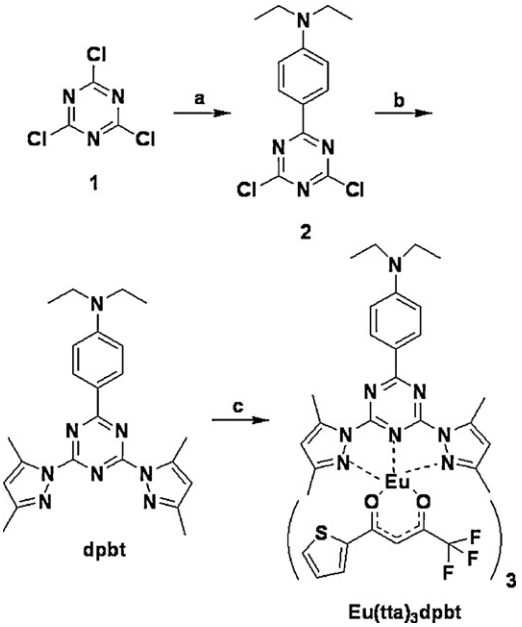

Scheme 6. Synthesis route for Eu(tta)$_3$dpbt. (a) *N*,*N*-diethylaniline; (b) potassium 3,5-dimethyl-pyrazolate; (c) Eu(tta)$_3$·3H$_2$O.
Scheme was reproduced from Ref. [28], with permission of the copyright holders.

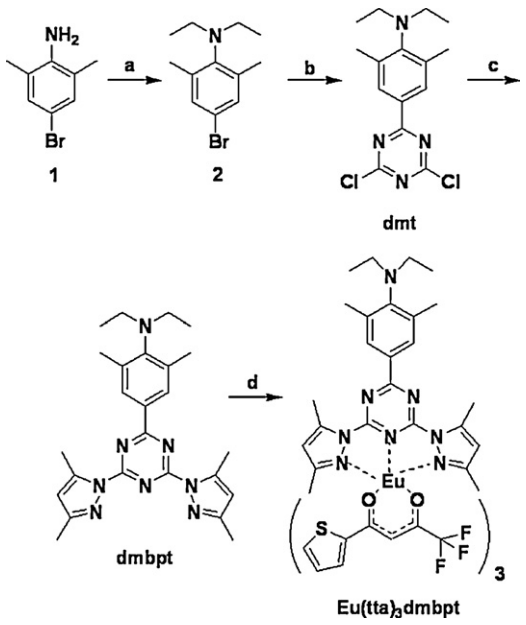

Scheme 7. Synthesis route for $Eu(tta)_3dmbpt$. (a) acetic acid, sodium borohydride; (b) *n*-butyllithium, cyanuric chloride; (c) potassium, 3,5-dimethylpyrazole; (d) $Eu(tta)_3{\cdot}3H_2O$.
Scheme was reproduced from Ref. [33], with permission of the copyright holders.

absorption peak in the visible region, derived from the absorptive transition of dmbpt, was much smaller than that of $Eu(tta)_3dpbt$. Although the one-photon absorbency of $Eu(tta)_3dmbpt$ in the visible region is lower than that of $Eu(tta)_3dpbt$, the twisted structure of dmbpt endows $Eu(tta)_3dmbpt$ with excellent two-photon-sensitized luminescent properties, which will be discussed in detail in Section 3.

Borisov and Wolfbeis studied the temperature dependence of the luminescence property of $Eu(tta)_3dpbt$, which possessed interesting potential to work as a temperature indicator [34a]. The decay times (τ) and the luminescence quantum yields (Φ) of $Eu(tta)_3dpbt$ were detected in the temperature region from 0 to 70 °C, and the τ value changed strongly with temperature decreasing. When dissolved in the air-saturated toluene, the τ value of $Eu(tta)_3dpbt$ was measured to be 480 μs at 25 °C and 620 μs at 1 °C. Accordingly, the Φ value was found to be 0.39 at 25 °C, but as high as 0.67 when the temperature decreased to 1 °C.

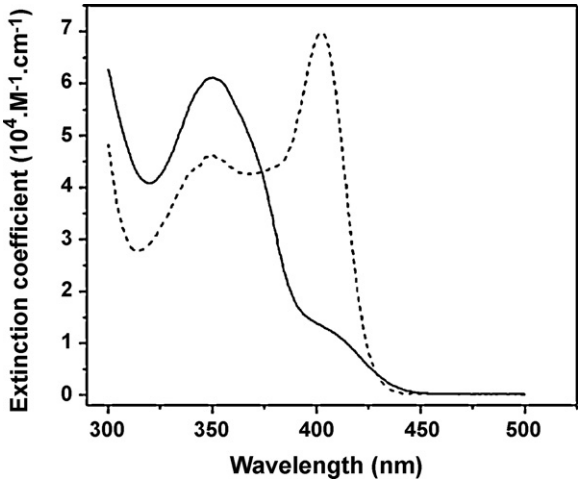

Fig. 3. UV/vis absorption spectra of $Eu(tta)_3dmbpt$ (—) and $Eu(tta)_3dpbt$ (- - -) in toluene (1×10^{-5} M).
Figure was reproduced from Ref. [33], with permission of the copyright holders.

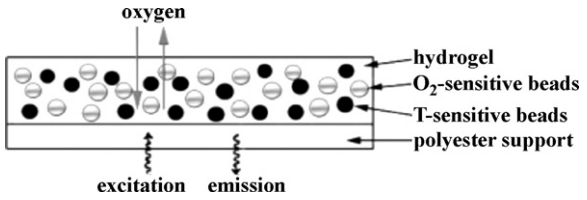

Fig. 4. Cross section of the sensor layer for simultaneous optical sensing of oxygen and temperature using bead-immobilized fluorescent probes dispersed in a hydrogel matrix.
Figure was reproduced from Ref. [34a], with permission of the copyright holders.

Microbeads composed of poly(4-tert-butyl styrene) (PTBS) and $Eu(tta)_3dpbt$ were prepared for developing a new kind of temperature sensor. The luminescence of the microbeads showed high photostability, and was not interfered with by oxygen. A luminescent temperature-oxygen bifunctional sensor, capable of being excited by a 405 nm LED, was created by dispersing the temperature-sensitive microparticles $Eu(tta)_3dpbt$/PTBS along with oxygen-sensitive microbeads composed of a palladium complex (palladium(II) 5,10,15,20-tetrakis(2,3,4,5,6-pentafluoro-phenyl)porphyrin, $\lambda_{em} = 680$ nm) and poly(styrene-co-acrylonitrile) in a thin layer of a hydrogel (Fig. 4). This sensor can be used for sensing the changes in oxygen concentration and temperature in humidified gas or aqueous media (Fig. 5).

Compared to the other reported dually sensing materials [34b,c], $Eu(tta)_3dpbt$/PTBS microbeads possesses the advantages of high brightness, narrow-line emission, and visible-light excitation.

Recently, we synthesized a new complex $Eu(tta)_3bpt$ (bpt = 2-(*N*,*N*-diethylanilin-4-yl)-4,6-bis(pyrazol-1-yl)-1,3,5-triazine, Scheme 8), in which, four hydrogen atoms replaced the methyl groups on the pyrazolyl rings in $Eu(tta)_3dpbt$ [35]. The change in structure endows $Eu(tta)_3bpt$ with enhanced long-wavelength sensitized luminescent properties at room temperature and a quite different emission spectrum. The $^5D_0 \rightarrow {}^7F_2$ transition of $Eu(tta)_3bpt$ splits into three peaks and the strongest emission line locates at 620 nm. However, for $Eu(tta)_3dpbt$, the $^5D_0 \rightarrow {}^7F_2$ transition exhibits two peaks, with the strongest emission line locating at 614 nm, which indicates the different surrounding symmetries around Eu^{III} ion between $Eu(tta)_3bpt$ and $Eu(tta)_3dpbt$.

Upon excitation at 410 nm, the luminescence quantum yield of $Eu(tta)_3bpt$ in toluene was measured at 295 K to be 0.43 using DCM in *n*-propanol as a reference, increasing by 23% relative to that of $Eu(tta)_3dpbt$ at the same temperature. It is interesting that the relationship between the luminescence quantum yields and temperature is linear for $Eu(tta)_3bpt$ but nonlinear for $Eu(tta)_3dpbt$. Although the exact cause of the different correlations between the luminescence quantum yield and temperature for the two complexes is unclear at present, $Eu(tta)_3bpt$ should have an advantage over $Eu(tta)_3dpbt$ for the preparation of luminescent temperature

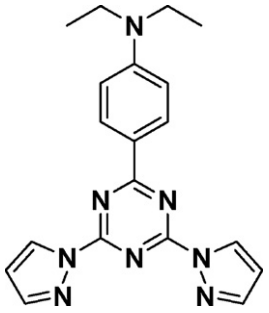

Scheme 8. Structure of ligand bpt.

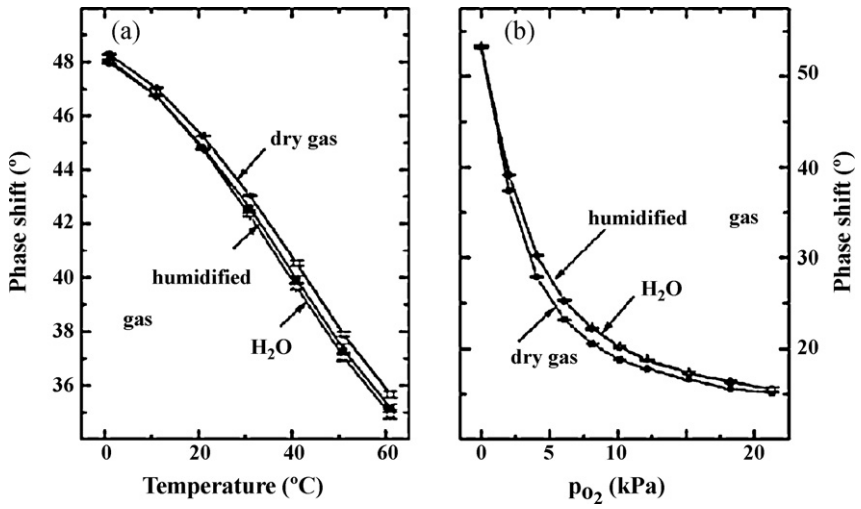

Fig. 5. Response of the dually sensor to temperature and oxygen in dry and humidified gases and in aqueous medium: (a) response to temperature (in the absence of oxygen) and (b) response to oxygen (at 25 °C).
Figure was reproduced from Ref. [34a], with permission of the copyright holders.

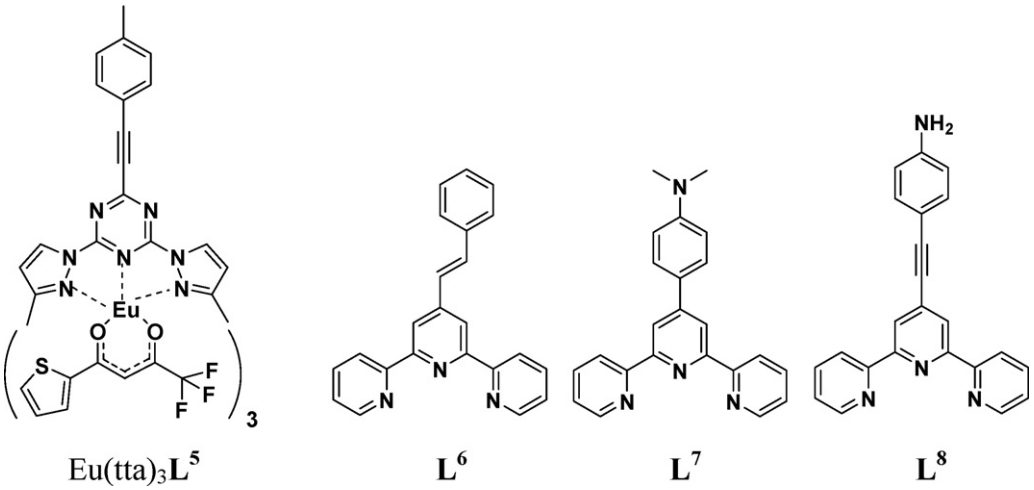

Scheme 9. Structure of the complexes Eu(tta)$_3$**L**^{n} (n = 5–8).

probes in view of the linear correlation. The different emitting-band shapes of Eu(tta)$_3$bpt and Eu(tta)$_3$dpbt and their high capabilities of long-wavelength sensitized luminescence may be applicable in developing new multiplex probes for bioanalysis.

The photophysical properties of the complexes Eu(tta)$_3$**L**^{n} (n = 5–8) (Scheme 9) were studied by Charbonnière and co-workers [36]. The electron-withdrawing group of ligand **L**^{5}, a bis-pyrazolyltriazine moiety, is similar to that in dpbt, while the electron-donating capability of the methyl group in **L**^{5} is much weaker than that of the diethylamino group in dpbt. An ethynyl spacer between the electron-donating and the electron-withdrawing moieties was introduced to extend electronic delocalization. Ligands **L**^{6} to **L**^{8} have the same terpyridine coordinating units as the electron-withdrawing groups, but the electron-donating groups and the π-bridge moieties are different.

Complexes Eu(tta)$_3$**L**^{5} and Eu(tta)$_3$**L**^{6} did not show absorption bands in the visible-light region. The low energy absorption bands of complexes Eu(tta)$_3$**L**^{7} and Eu(tta)$_3$**L**^{8} appeared as shoulders of the high energy ones, and reached the visible region. The Eu^{III} luminescence quantum yields of Eu(tta)$_3$**L**^{5} (1.4%), Eu(tta)$_3$**L**^{6} (2.8%), and Eu(tta)$_3$**L**^{8} (5.9%) were much lower compared to that of Eu(tta)$_3$**L**^{7} (20.0%) in which the central pyridine ring of the terpyridine is directly linked with the amino-substituted phenyl ring.

More recently, a new kind of Eu^{III} complex, Eu(tta)$_4$·DEASPI with a possible structure as shown in Scheme 10 was reported by Wang and co-workers [37]. In the absorption spectrum of Eu(tta)$_4$·DEASPI, two absorption bands around 340 nm and 485 nm

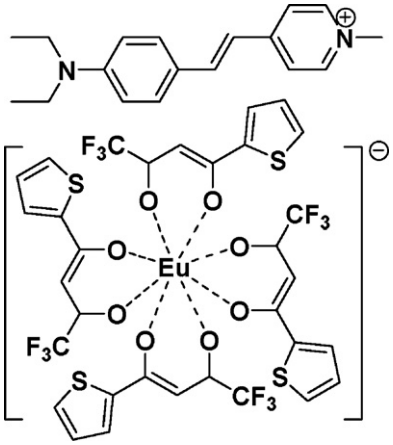

Scheme 10. Structure of the complex Eu(tta)$_4$·DEASPI.

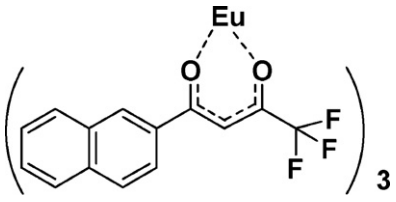

Scheme 11. Structure of complex Eu(nta)$_3$.

were observed. The ultraviolet absorption band is attributed to the absorption of tta [38], and the band in the visible region with the tail extending beyond 550 nm is derived from DEASPI. The absorption band of the sensitizer DEASPI did not show any red-shift after forming the complex with Eu(tta)$_4^-$, which also indicated that DEASPI did not coordinate directly to Eu^{III} ion in this complex. The molar extinction coefficient of DEASPI in Eu(tta)$_4$·DEASPI has the same order of magnitude with tta. However, upon excitation at 485 nm, the emission of Eu^{III} ion ($^5D_0 \rightarrow {}^7F_2$ transition) and a broad fluorescence band of DEASPI appeared in the same wavelength region, resulting in difficulty in estimating the Eu^{III} luminescence efficiency of this complex upon long-wavelength sensitization from the reported data.

The luminescent properties of dpbt-sensitized Eu^{III} complexes are obviously influenced by the supplementary ligands. It was reported that the quantum yields and lifetimes of the Eu^{III} luminescence of Eu(nta)$_3$dpbt (nta = naphthoyltrifluoroacetone, Scheme 11) and Eu(fod)$_3$dpbt were quite different from those of Eu(tta)$_3$dpbt [34]. The luminescent quantum yields (λ_{ex} = 410 nm, 298 K) were 0.52, 0.42, and 0.39 for Eu(nta)$_3$dpbt, Eu(fod)$_3$dpbt, and Eu(tta)$_3$dpbt, respectively, and the decay times in air-saturated toluene at 298 K were 430, 560, and 480 μs, respectively. It is likely that the supplementary β-diketonate ligands in the dpbt-sensitized Eu^{III} complexes have an important influence on the energy-transfer efficiency from dpbt to Eu^{III} ion.

2.2. Singlet energy-transfer pathway

The singlet energy-transfer pathway in which the energetic constraints from the T_1 state of the ligand can be avoided is an effective strategy for the development of long-wavelength-sensitized Ln^{III} complexes with high sensitization efficiencies. However, few lanthanide complexes especially those of the Eu^{III} ion, capable of being efficiently sensitized through a singlet pathway are known.

The research on the singlet energy-transfer mechanism in luminescent lanthanide complexes was conducted in two ways. One was conducted by virtue of indirect evidences such as the phosphorescent dependency on oxygen concentration, and the similar external heavy-atom effect of Ln^{III} ions on the ligand fluorescence and phosphorescence; while the other is based on finding direct evidence from the excited-state dynamics of the lanthanide complexes.

The complexes demonstrated to be sensitized through the singlet energy-transfer pathway by means of direct evidence on the excited-state dynamics are rare. This may be due to the following two facts: first, lanthanide complexes in which the single energy-transfers pathway dominates the sensitization of lanthanide ions have been very limited; secondly, with such complexes, there was difficulty in measuring the decay dynamics of S_1 and T_1 states of coordinated chromophores as well as the population rise dynamics of the lanthanide luminescent states.

The first reliable direct evidence of excited-state dynamics for the singlet pathway-dominated excitation energy-transfer from the antenna ligand to the Ln^{III} ion in a lanthanide complex was obtained on Eu(tta)$_3$dpbt [28].

First, on the nanosecond timescale (Fig. 6(a)), the $S_1 \rightarrow S_0$ fluorescence emission of the coordinated ligand dpbt centered at 430 nm with a decay time constant of 1.3 ns was observed. Simultaneously, the rise-time constant of the emission corresponding to the $^5D_1 \rightarrow {}^7F_3$ transition of the Eu^{III} ion at 585 nm was 1.8 ns. This decay-to-rise correlation clearly revealed the singlet transfer pathway of the excitation energy in Eu(tta)$_3$dpbt. Secondly, on the sub-microsecond timescale (Fig. 6(b)), a tight correlation between the decay of the $^5D_1 \rightarrow {}^7F_{1-3}$ luminescence signals at 535, 555, and 585 nm (decay constant, 387 ns) and the rise of the $^5D_0 \rightarrow {}^7F_2$ luminescence at 614 nm (rise constant, 392 ns) was established. This indicates the transfer of the excited-state population from the $^5D_1$ state to the $^5D_0$ state of the Eu^{III} ion. The lifetime of the excited-state $^5D_0$ was 0.48 and 0.65 ms at room temperature and 77 K, respectively (Fig. 6(c)).

Thirdly, the time-resolved phosphorescence spectrum of Eu(tta)$_3$dpbt (the inset of Fig. 6(d)) measured at 77 K and after a delay time of 1 s revealed an asymmetric broad phosphorescence band centered at around 525 nm that was derived from the T_1–S_0 transition of the coordinated dpbt. The lifetime of the T_1 state of the coordinated dpbt was 3.9 s, which is significantly longer than the lifetime of the $^5D_0$ state of the Eu^{III} ion in the complex at 77 K (0.65 ms). Moreover, in the insert of Fig. 6(d), a weak remnant of emission at 614 nm was also recorded. Therefore, in Eu(tta)$_3$dpbt, the excitation energy transfer from dpbt to Eu^{III} ion occurred dominantly through a singlet pathway, while the probability of that through the triplet pathway, if any, was very low ($<10^{-3}$) as illustrated in Fig. 7.

The detailed steps in the singlet energy-transfer pathway are still an open question. A ligand-to-Eu^{III} charge transfer state might be involved in this process. The strong coupling between the excited-state S_1 of dpbt and some energy level of the Eu^{III} ion should be important for breaking the forbidden character of the 4*f*–4*f* transition of Eu^{III} ion in Eu(tta)$_3$dpbt, which makes it possible to populate the excited-state of Eu^{III} ion immediately after the excitation of dpbt. With the excitation energy transferring from dpbt to the luminescent state of Eu^{III} ion via the singlet pathway and the excited electron of dpbt dropping to the ground state, the forbidden character of the 4*f*–4*f* transition is partly recovered. As a result, the radiative deactivation process is much slower than the sensitization process of the Eu^{III} ion. The time-resolved spectra study in the picosecond timescale with high resolution and sensitivity would be helpful for further understanding the details of the singlet pathway mechanism.

On the other hand, several studies regarding the indirect evidence for the singlet energy-transfer pathway in NIR-emitting lanthanide complexes have been reported [30,39–41]. The photophysical properties of six different Ln^{III} complexes with the same dendritic ligand, which contains 21 amide groups in the interior and 24 dansyl units in the periphery were reported in 2002 [30], and the sensitization mechanism was studied for each Ln^{III} complex. In the case of Nd^{III} complex, a singlet energy-transfer pathway was supported by the extensive overlap between the fluorescence emission band of the ligand and the energy level of Nd^{III} ion.

In the same year, two Nd^{III} complexes with dansyl and lissamine fluorescent dyes (Scheme 12) as the sensitizers for Nd^{III} luminescence were reported. A singlet pathway for the sensitization of the Nd^{III} luminescence in complexes containing dansyl- and lissamine-chromophores which were not directly coordinated to Nd^{III} ion was demonstrated by several experimental results [39].

Gd^{III} ion in the complexes cannot accept any excitation energy from the triplet and singlet states of the lissamine and dansyl groups, because Gd^{III} ion has no energy gap for f–f transition below 32,000 cm^{-1}, which was much higher than the levels of the triplet and singlet states of the sensitizers. The complexes Gd**L**^{9} and Gd**L**^{10} could thus be used as models to study the fluorescence of sen-

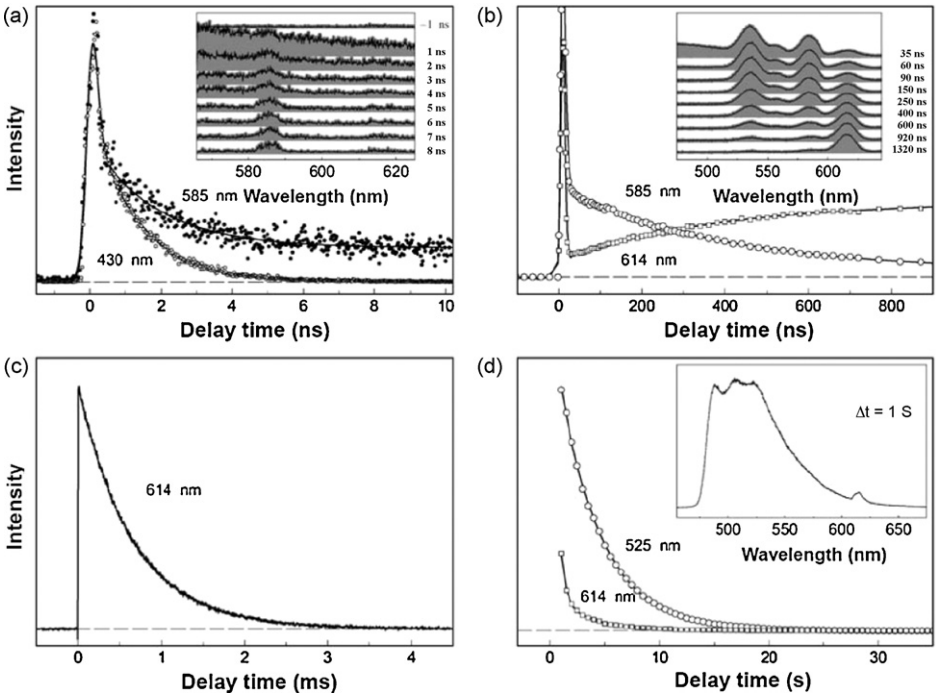

Fig. 6. The time-resolved luminescence spectra of Eu(tta)$_3$dpbt in toluene at room temperature (a and b) and 77 K (c and d). (a) Kinetic curves at 430 nm (◯) and 585 nm (●) with an excitation pulse at 400 nm (130 fs); the inset shows the luminescence spectra at different delay times (t_d). (b) Kinetic curves at 585 nm (◯) and 614 nm (□) with an excitation pulse at 417 nm (5 ns); the inset shows the luminescence spectra at different delay times. (c) Kinetic curves at 614 nm with an excitation pulse at 417 nm (5 ns). (d) Kinetic curves at 525 nm (◯) and 614 nm (□); the inset shows the phosphorescence spectrum of complex 4 after a delay time of 1 s.
Figure was reproduced from Ref. [28], with permission of the copyright holders.

sitizers in the presence of a lanthanide ion, but in the absence of energy transfer. The fact that the fluorescence quantum yield and lifetime of the ligands in the Gd^{III} complexes were close to those of the free ligands indicated that the lanthanide ions cannot provide an external heavy-atom effect on the luminescent properties of lissamine and dansyl units and the population of the triplet states in these complexes was not significant. Based on the aforementioned experimental results, the reduction of the fluorescence lifetimes and quantum yields of the coordinated ligands in the Nd^{III} complexes with respect to those of the free ligands (Table 1) was considered to be the evidence of the direct energy transfer from the sensitizers' excited singlet state to the luminescent state of Nd^{III} ion in these complexes.

Moreover, oxygen may decrease the quantum yield of lanthanide luminescence of complexes that possess a triplet energy-transfer pathway because the excited triplet state can be

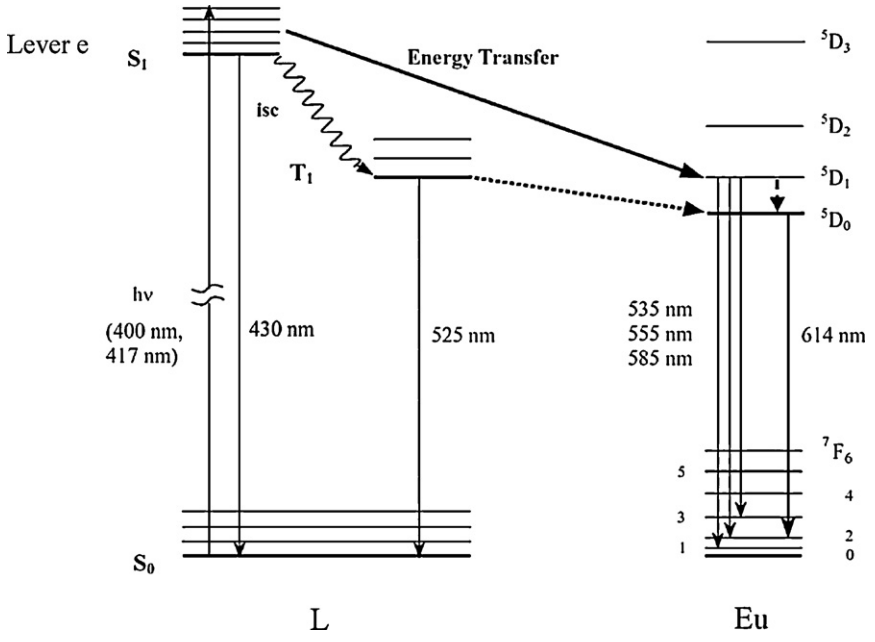

Fig. 7. Energy level diagram showing the energy-transfer pathways in Eu(tta)3dpbt.
Figure was reproduced from Ref. [28], with permission of the copyright holders.

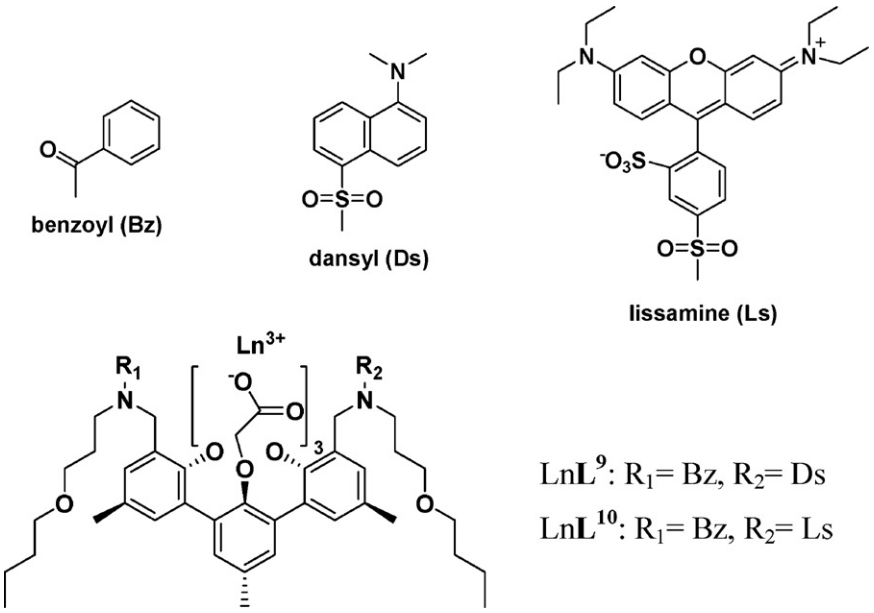

Scheme 12. Structures of the complexes, dansyl-functionalized lanthanide complex (Ln**L**^{9}) and lissamine-functionalized lanthanide complex (Ln**L**^{10}).

quenched by oxygen [41,42]. The luminescence intensities of the complexes Nd**L**^{9} and Nd**L**^{10} did not increase after the deoxygenation of the sample, implying that the triplet state did not play an important role in the energy-transfer process.

The author speculated that the presence of tertiary amine groups which have the quadrupole moments in dansyl and lissamine units may be the reason for the highly forbidden character of the $S_1 \rightarrow T_1$ transition, so that the singlet energy-transfer processes take place in Nd**L**^{9} and Nd**L**^{10}.

Comparison of the structures and excitation energy-transfer processes of Nd**L**^{9} and Nd**L**^{10} with those of Eu(tta)$_3$dpbt may provide an interesting approach to understanding the singlet pathway. We believe that the mechanisms of the singlet energy-transfer pathways in Nd**L**^{9}/Nd**L**^{10} and Eu(tta)$_3$dpbt are different, i.e. the requirements are different for the antenna ligands of Nd**L**^{9}/Nd**L**^{10} and Eu(tta)$_3$dpbt to promote the energy transfer via a singlet pathway, although the inactive $S_1 \rightarrow T_1$ transition feature is the same for the both cases. The excitation of the 4*f*–4*f* electronic transition of Nd^{III} ion in Nd**L**^{9} and Nd**L**^{10} only needs the breakdown of the parity selection rules, but the excitation of Eu^{III} ion in Eu(tta)$_3$dpbt needs to relax both of the parity selection rules and the electron spin selection rules.

3. Two-photon-sensitized emission of europium complexes

Two-photon excitation (TPE) means simultaneous absorption of two photons, accompanied by the transition of an absorbing molecule from a lower energy level to a higher level [43]. TPE allows molecules that absorb light in the ultraviolet region to be excited with red or near-infrared light, which is an attractive way to promote a molecule to an excited-state for various applications including at least the optical storage [44a], optical limitation [44b], microfabrication [45], bioimaging [46a], and photodynamic therapy [46b]. Most of the commercially available two-photon dyes are organic compounds [47] with broad emission bands and short luminescence lifetimes in the nanosecond scale, which limit the sensitivity of bioanalysis or bioimaging based on such label materials due to the autofluorescence of biosamples.

Table 1
Fluorescence lifetimes (τ) and fluorescence quantum yields (Φ) of the complexes Ln**L**^{9} and Ln**L**^{10} in DMSO solution.

	L^{9}	Gd**L**^{9}	Nd**L**^{9}	**L**^{10}	Gd**L**^{10}	Nd**L**^{10}
τ [ns]	16.2	16.2	2.75	2.92	2.85	1.67
Φ[a]	0.66	0.61	0.12	0.75	0.78	0.27

[a] The experimental error on Φ is 10%.

The two-photon-sensitized luminescence of lanthanide complexes is aroused via the TPE of a light-harvesting antenna ligands and subsequent excitation energy transfer (EET) to the metal ions. The efficiency of two-photon-sensitized luminescence of Ln^{III} complex can be reflected by the value of TPE action cross section, $\delta\Phi^{L}_{Ln}$, where δ is the two-photon absorption (TPA) cross section.

TPE provides a very promising manner for extending the excitation windows of lanthanide complexes to the red or near-infrared (NIR) light wavelength region [48–50]. It is expected that fluorescent immunoassay or bioimaging techniques based on such a lanthanide luminescence label material, capable of being efficiently excited by NIR laser radiation, will combine the advantages of high sensitivity, high signal-to-noise ratio, deep penetration, and low photodamage to biological samples. However, the number of known lanthanide complexes with excellent TPE-sensitized luminescence properties is still very limited [3,33,48,50–54].

The two-photon excited luminescence of lanthanide complexes was first observed experimentally in a crystal containing divalent europium ions under excitation with a ruby laser [55]. In 2001, the direct multiphoton excitation with a Ti:sapphire laser of lanthanide ions in D_2O was reported by Lakowicz et al. for the first time [56]. However, the emission intensities were weak upon the direct multiphoton excitation of the lanthanide ions. The multiphoton excitation of lanthanide ions coordinated with nucleic acids, proteins and fluorescent chelators was also explored by the same group. In these cases, excitation occurred by multiphoton absorption of the sensitizers [51,52], however, no cross sections of multiphoton absorption were given.

It has been an important pursuit to design and synthesize novel lanthanide complexes possessing high efficiencies for two-photon sensitized luminescence. Multiphoton excitation of Tb^{III} ion bound to the transferrin protein was reported by Thomson and coworkers. The photons' energy, with wavelengths of 503 and 566 nm for two-photon excitation and 800 nm for three-photon excitation, was absorbed by tyrosine residues in a protein and the excitation

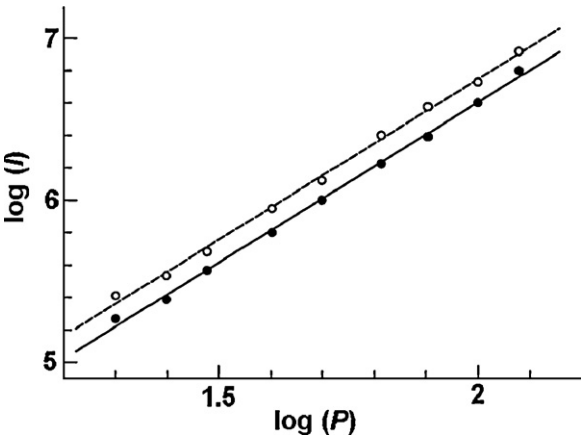

Fig. 8. TPE-sensitized luminescence intensity (I) versus the incident laser power (P) for free dpbt (○; λ_{ex} = 745 nm, λ_{em} = 405 nm) and Eu(tta)$_3$dpbt (●; λ_{ex} = 799 nm, λ_{em} = 614 nm) in toluene. The slopes of the lines are both 1.98 ± 0.04.
Figure was reproduced from Ref. [48], with permission of the copyright holders.

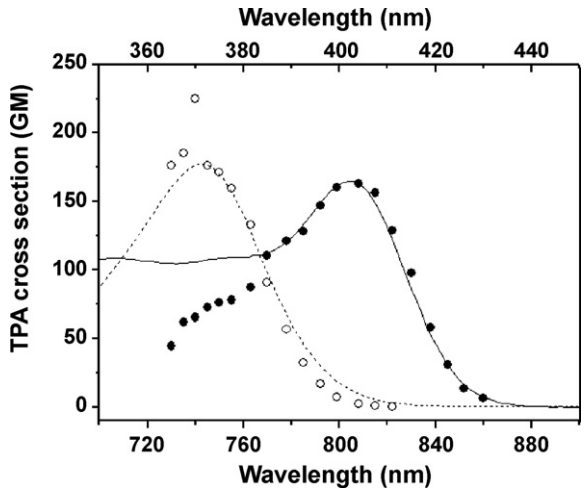

Fig. 9. TPA cross sections (δ) for Eu(tta)$_3$dpbt (●; λ_{em} = 614 nm) and dpbt (○; λ_{em} = 405 nm) in toluene (1×10^{-4} M). The one-photon-absorption spectra of Eu(tta)$_3$dpbt (solid line) and dpbt (dash line) are shown using the upper abscissa to reflect the relationship between the wavelength-doubled one-photon absorption spectra and the TPE spectra. The peak intensities are arbitrarily scaled.
Figure was adapted from Ref. [48], with permission of the copyright holders.

energy subsequently transferred to the lanthanide ions [49,57]. The action cross section for the direct two-photon excitation of Tb^{III} luminescence using 566 nm pulses laser amounted to 10^{-5} GM (1 GM = 10^{-50} cm^4 s photon^{-1} molecule^{-1}), while the action cross sections for the two-photon excitation of transferrin-sensitized Tb^{III} luminescence were 0.4 GM under excitation at 566 nm, and 7.4 GM at 503 nm, respectively, which were five orders of magnitude higher than that of directly excited Tb^{III} luminescence. However, the two-photon sensitization efficiency was still low for real applications.

The TPE-sensitized Eu^{III} luminescence is of significance for developing bioanalysis or bioimaging technologies due to the acceptable red-light penetrability of biosamples. Eu(tta)$_3$dpbt exhibited striking two-photon-sensitized Eu^{III} luminescence properties, with a maximum TPA cross sections of 157 GM upon the excitation at 808 nm and a corresponding $\delta \times \Phi_F$ value of 82 GM [48]. The TPE processes of free dpbt and Eu(tta)$_3$dpbt were confirmed by the power dependence experiments (Fig. 8).

The two-photon-absorption (TPA) cross sections of free dpbt in toluene, with a maximum value of 185 GM, was measured in the spectroscopic region of 730–830 nm using femtosecond laser pulses (Fig. 9). The fluorescence excitation spectrum of dpbt in toluene is identical to the one-photon-absorption spectrum. The absorption and fluorescence spectra display a perfect mirror–image relationship, indicating the similar molecular configurations of dpbt in the S_0 and S_1 states.

The strong intramolecular charge transfer (ICT) character of the S_1 state and the considerable large transition dipole moment are significant bases for an efficient two-photon absorber [58]. dpbt is a polar chromophore which possesses a D-π-A structure, with the *N*,*N*-diethylaniline group as an electron-donor (D) and the dipyrazolyltriazine moiety as an electron acceptor (A). The ICT character of the S_1 state of dpbt was reflected by the spectroscopic data (linear absorption and fluorescence) of dpbt in six organic solvents with different polarities (Table 2) and was strongly supported by a theoretical calculation on molecular orbitals.

It can be seen from Table 2, upon increasing the solvent polarity, the absorption and the fluorescence maximum wavelengths exhibit bathochromic shifts and the Stokes shift increases in parallel, whereas the fluorescence quantum yield drops significantly. These spectroscopic features reflect the ICT character of S_1 state [59].

The theoretical calculations conducted on dpbt clearly indicated that the lowest-energy transition presents a marked CT character, with a significant change in the electron-density distribution over the diethylaniline and the dipyrazolyltriazine moieties between the HOMO and LUMO of dpbt (Fig. 10).

The TPE luminescence of Eu(tta)$_3$dpbt at 614 nm was mainly attributed to the sensitization effect of coordinated dpbt rather than that of tta because in the spectroscopic region below 380 nm, the two-photon-excitation spectrum deviates significantly from the wavelength-doubled one-photon absorption of coordinated tta (Fig. 9). In the wavelength regions from 760 to 820 nm for Eu(tta)$_3$dpbt and 740 to 820 nm for free dpbp, the experimental data of the TPA spectra agree well with the wavelength-doubled linear absorption spectra. These results suggest that the S_1 state is both one- and two-photon allowed, and the singlet energy-transfer mechanism is in operation also for the two-photon-sensitized Eu^{III} luminescence in Eu(tta)$_3$dpbt.

A europium complex Eu(tta)$_3$dmbpt (Scheme 5) that we reported later [33] also exhibited excellent two-photon-sensitized luminescent properties. The maximum $\delta \times \Phi_F$ value was determined to be 85 GM at 812 nm for Eu(tta)$_3$dmbpt (Fig. 11), and the TPE window is markedly red-shifted with respect to that of Eu(tta)$_3$dpbt. For example, the $\delta \times \Phi_F$ value of Eu(tta)$_3$dmbpt is as high as 56 GM at 842 nm, while that of Eu(tta)$_3$dpbt is about 20 GM.

The maximum TPA cross section of free dmbpt in toluene is 206 GM at 729 nm and the TPE window extends up to 842 nm (Fig. 12), although the molar extinction coefficient measured in the linear absorption spectrum of dmbpt in toluene (0.9×10^4 M^{-1} cm^{-1}, λ_a = 361 nm) is much lower than that of dpbt (4.7×10^4 M^{-1} cm^{-1}, λ_a = 374 nm), which may derive from the large

Table 2
Absorption and fluorescence maximum wavelengths (λ_a and λ_{em}), Stokes shift $\Delta\lambda$, and fluorescence quantum yields (Φ_F) of dpbt dissolved in organic solvents with a polarity factor $P(\varepsilon)$.

Solvent	$P(\varepsilon)$[a]	λ_a [nm]	λ_{em} [nm]	$\Delta\lambda$ [nm][b]	Φ_F
DMF	0.922	381	444	63	0.03
Ethanol	0.886	384	440	56	0.02
Tetrahydrofuran	0.687	378	422	44	0.27
Diethyl ether	0.526	370	404	34	0.67
Toluene	0.343	374	405	31	0.75
n-Hexane	0.229	368	375	7	0.81[c]

[a] Polarity factor is defined as $P(\varepsilon) = (\varepsilon - 1)/(\varepsilon + 2)$, where ε is the dielectric constant.
[b] Stokes shift is defined as $\Delta\lambda = \lambda_{em} - \lambda_a$.
[c] Poor solubility in this solvent.

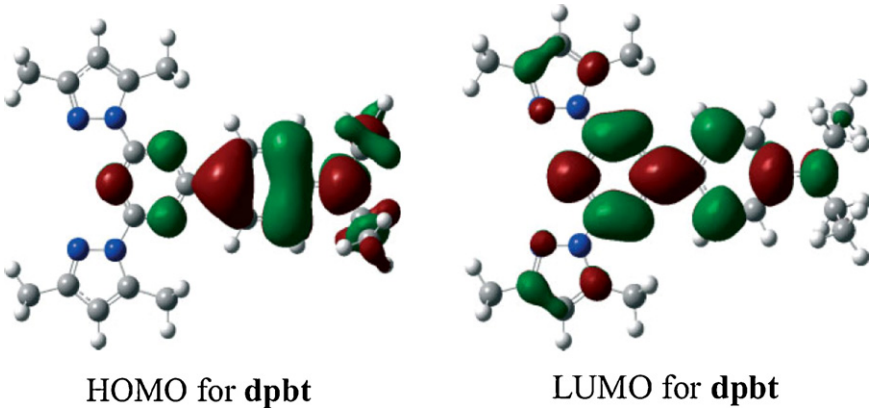

Fig. 10. Frontier orbitals of HOMO and LUMO for dpbt. The geometry optimization and the frontier orbital population analysis were performed at the B3LYP/6-31G level. All calculations were carried out by using the GAUSSIAN03 program package.
Figure was adapted from Ref. [33], with permission of the copyright holders.

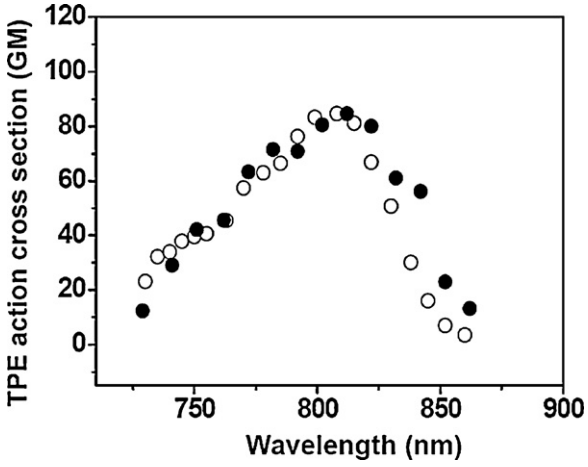

Fig. 11. Action cross sections of TPE fluorescence ($\delta \times \Phi_F$) for Eu(tta)3dmbpt (filled circles) and Eu(tta)3dpbt (open circles) in toluene (1.0×10^{-4} M). The experimental uncertainty on δ is 10–15%.
Figure was adapted from Ref. [33], with permission of the copyright holders.

difference in the configurations between the ground state and the excited-state of dmbpt.

For asymmetrical D-π-A type polar chromophores, the TPA cross section can be related to the difference in static dipole moment

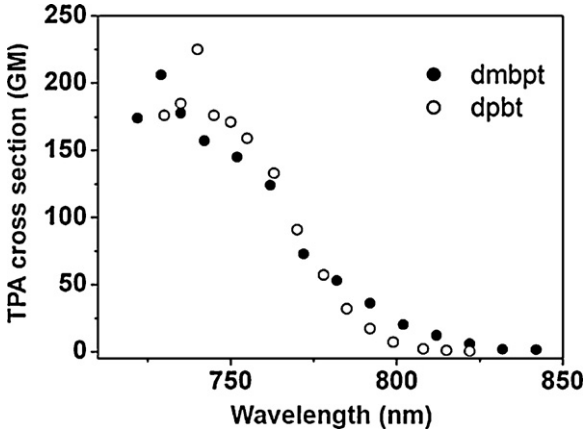

Fig. 12. Two-photon absorption cross sections (δ) for dmbpt and dpbt in toluene (1.0×10^{-4} M). The experimental uncertainty on δ is 10–15%.
Figure was reproduced from Ref. [33], with permission of the copyright holders.

($\Delta\mu$) and the transition dipole moment (M_{01}) between the S_0 and the S_1 state, as well as the detuning energy ΔE ($\Delta E = E_{ge} - \hbar\omega$), where E_{ge} stands for the transition energy between S_0 and S_1, ω is the fundamental frequency of light, and $\hbar$ is Planck's constant [58d,f,60]:

$$\delta \propto \frac{M_{01}\Delta\mu}{\Delta E} \quad (2)$$

A large value of $\Delta\mu$ M_{01} and a small value of ΔE would facilitate the probability of a two-photon absorptive transition. Based on the electronic absorption spectra, the $S_0 \rightarrow S_1$ transition dipole moment M_{01} for dmbpt was estimated to be 3.6 D, which is less than that for dpbt (6.9 D), and the detuning energy for dmbpt was estimated to be 1.72 eV, which is a little bigger than that for dpbt (1.65 eV). However, a calculation according to the reported method [61] indicated that $\Delta\mu$ of dmbpt is 15.4 D, which is larger than that of dpbt (9.4 D). Therefore, it is obviousl that the large $\Delta\mu$ is chiefly responsible for the large TPA cross section of dmbpt.

Further investigation on the molecular structure of dmbpt described in the Section 2.1 revealed that the large $\Delta\mu$ value may derive from the twisted structure of dmbpt. The 2,6-dimethyl substitutes in dmbpt bring about a significant twist in the conformation of the diethylamino group compared to that in dpbt, which severely influences the conjugation in the ground state between the electron lone-pair of N in the $-N(CH_2-)_2$ moiety and the aromatic electron system in dmbpt.

The fairly large $\Delta\mu$ of dmbpt can be explained based on the theoretical calculation results for the frontier orbitals of dmbpt (Fig. 13). Compared with the results for dpbt (Fig. 10), the electron cloud on HOMO in dmbpt tends to more densely distribute on the diethylamino moiety, owing to the severely twisted $-N(CH_2-)_2$ group and the influence of 2,6-dimethyl groups on the phenyl ring in dmbpt. The electron-density distribution of LUMO in dmbpt is quite similar to that in dpbt.

For complexes, $Eu(tta)_3$dmbpt exhibits much better TPE-sensitized luminescent properties than $Eu(tta)_3$dpbt in the long-wavelength NIR region, which could be partly attributed to the smaller band gap between HOMO and LUMO for coordinated dmbpt than that for coordinated dpbt. After coordinating to Eu^{III} ion, the influence of the Eu^{III} electric field on the HOMO electron cloud of dpbt should be stronger than that of dmbpt, owing to the holistic conjugated structure of dpbt. While, the influence of the Eu^{III} ion electric field on the LUMO electron clouds of coordinated dmbpt and dpbt is similar as most parts of the excited electron clouds are similarly distributed on the two different molecules. Therefore the Eu^{III} ion electric field induced decrease in the HOMO–LUMO energy gap of dmbpt is larger than that of dpbt.

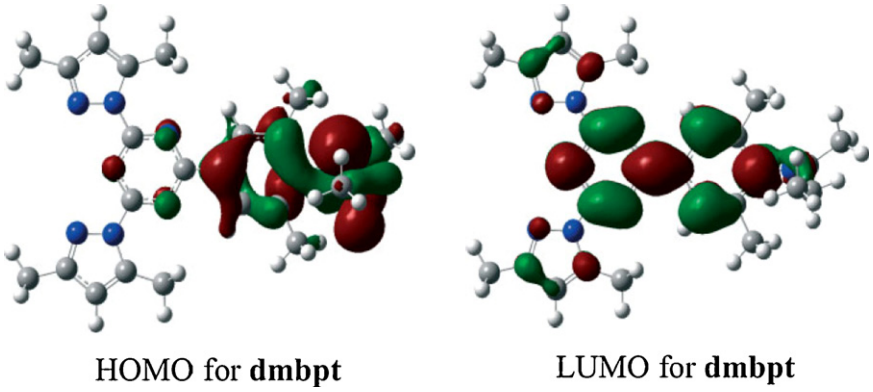

Fig. 13. Frontier orbitals of HOMO and LUMO for dmbpt. The geometry optimization and the frontier orbital population analysis were performed at the B3LYP/6-31G level. All calculations were carried out by using the GAUSSIAN03 program package.
Figure was adapted from Ref. [33], with permission of the copyright holders.

The two-photon-sensitized luminescence properties of the MK-Eu(Fod)$_3$ complex in a toluene solution (Eu(fod)$_3$/Michler's ketone ratio: 10) was reported by Werts et al. in 2005 [54]. The strong CT character of MK in MK-Eu(Fod)$_3$ makes it a good candidate for two-photon absorber. The two-photon absorption cross section of MK-Eu(Fod)$_3$ (δ_{max} = 253 GM, λ_{ex}: 810 nm) is much higher than that of Eu(tta)$_3$dpbt. However, its TPE action cross section is smaller than that of Eu(tta)$_3$dpbt with a $\delta \times \Phi_F$ value of 43 GM owing to its relatively low luminescence quantum yield.

A series of D_3 symmetric octupolar structural Eu^{III} complexes were designed by Maury and co-workers [50]. A dicarboxamide pyridine-based chromophore **L^{11}** presented marked CT character upon excitation, and the complex [Eu**L^{11}**$_3$][OTf]$_3$ (Scheme 13) exhibited a good two-photon absorption capability with a maximum TPA cross section of 96 GM at 720 nm. However, the efficiency of two-photon-sensitized Eu^{III} luminescence of [Eu**L^{11}**$_3$][OTf]$_3$, with a $\delta \times \Phi_F$ value of 5.4 GM, was suppressed by its low luminescence quantum yield (0.056).

For applications in bioimaging and bioassay [62–64], it is important to develop lanthanide complexes which are soluble and stable in aqueous media and have considerable TPE action cross sections upon the excitation in the water-window spectroscopic region.

In 2008, a complex Na$_3$[Eu**L^{12}**$_3$] (Scheme 14) which is stable and soluble in organic solvents and water was reported by Maury and co-workers [62]. Pyridine dicarboxylic acid (DPA) and its analogous were known to be sufficiently stable in water for most of spectroscopic studies [65,66], hence a derivative of DPA with a D-π-A structure and a hydrosoluble tail of 3,4,5-tris(triethylene-glycol)phenyl (HG) [47,67] was adopted in this complex. The maximum TPA cross section in the spectroscopic range of 700–900 nm is about 92 GM (λ_{ex}: 700 nm), and the luminescence quantum yield of this complex is about 15.7%, which gives a maximum $\delta \times \Phi_F$ value of 15 GM.

Using Na$_3$[Eu**L^{12}**$_3$] in a PBS solution as a probe, a two-photon scanning microscopy bioimaging experiment for T24 cancer cells was carried out. The luminescence image (Fig. 14, left) was taken on a biphotonic laser scanning microscope upon femtosecond 760 nm irradiation (δ_{TPA} = 19 GM at 760 nm). Comparison between the luminescence image and a phase contrast image (Fig. 14, right) clearly indicated that the complex was mainly localized in a perinuclear region and its distribution is similar to that of the endoplasmic reticulum. In addition, bright spots can be observed in the nucleus, implying that the complex preferentially targeted small organelles called nucleoli.

A series of new europium complexes (Scheme 15) was reported later [64], and the CT character of the ligands and the TPA cross sections of these complexes can be tuned by changing the donor group, such as dialkylamino, alkoxy, and alkylthio, as well as the length of the π-conjugated backbone, such as phenyl, phenylethynyl, naphtylethynyl, bis(phenylethynyl), and chalcone.

[NBu$_4$]$_3$[Eu**L^{13}**$_3$] exhibited the largest δ_{max} value in these complexes, about 775 GM at 740 nm, the highest value ever reported for

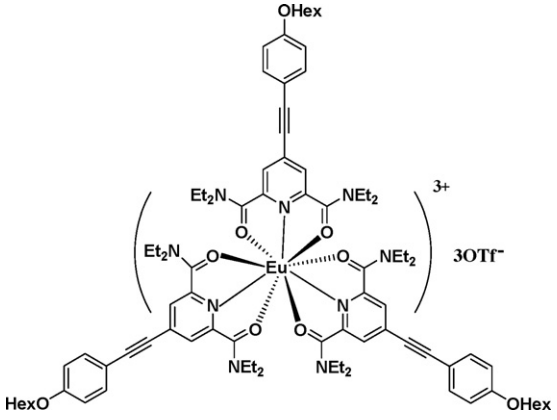

Scheme 13. Structure of the complex [Eu**L^{11}**$_3$][OTf]$_3$.

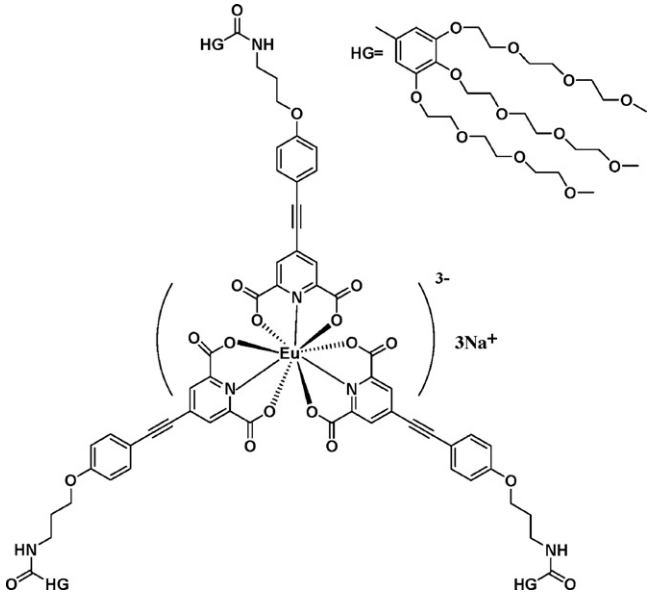

Scheme 14. Structure of complex.

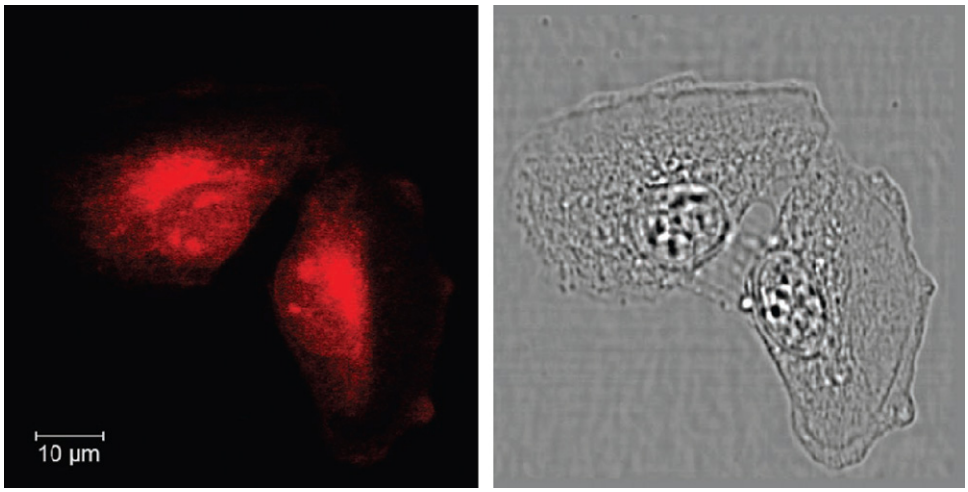

Fig. 14. Two-photon excited luminescence (left, λ_{ex} = 760 nm) and phase contrast (right) images of T24 cancer cell fixed in ethanol and loaded with $Na_3[Eu\mathbf{L}^{12}{}_3]$. Figure was reproduced from Ref. [62], with permission of the copyright holders.

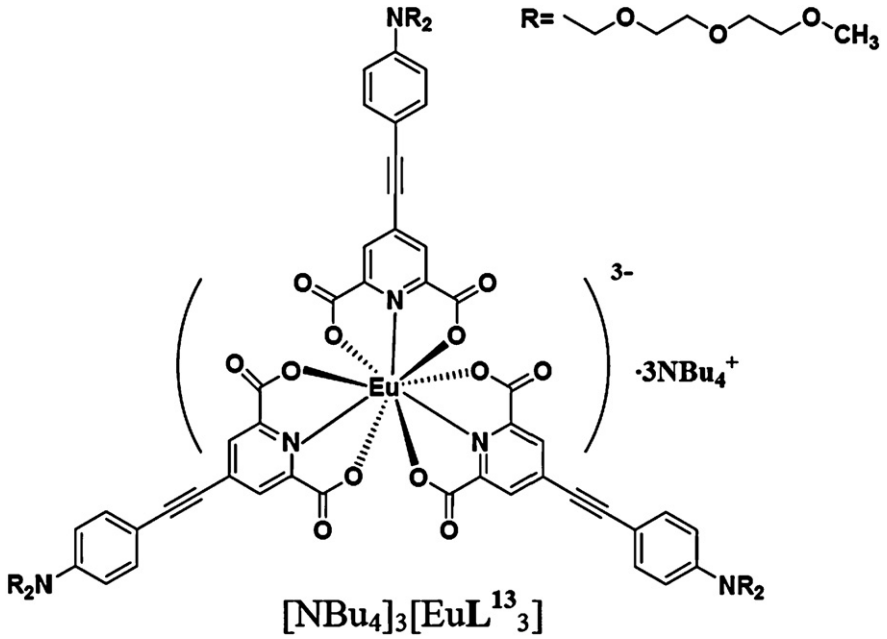

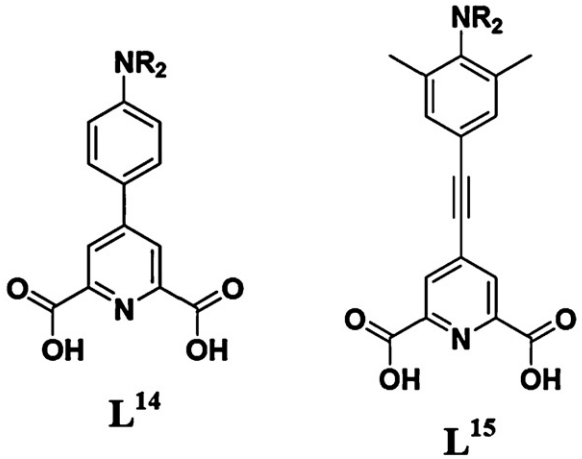

Scheme 15. Structure of complexes $[NBu_4]_3[Eu\mathbf{L}^n{}_3]$ (n = 13–15).

a Eu^{III} complexes, which indicated that the ligand $\mathbf{L^{13}}$ was an excellent two-photon absorber. The large δ_{max} value of $[NBu_4]_3[Eu\mathbf{L^{13}}_3]$ could be attributed to the strong electron-donor group (dialkylamino group) and the large π-conjugated backbone of $\mathbf{L^{13}}$. Although the luminescence quantum yield of $[NBu_4]_3[Eu\mathbf{L^{13}}_3]$ is low ($\Phi = 0.070$), a $\delta \times \Phi_F$ value of about 52 GM is an exhilarating two-photon-sensitized luminescence property of the water soluble Eu^{III} complex.

The authors demonstrated that reducing the extent of π-conjugation in the antenna ligand would result in a significant decrease of the TPA cross section. As shown in Scheme 14, $\mathbf{L^{14}}$ was the ligand obtained through shorting the π-skeleton of $\mathbf{L^{13}}$, and the $\mathbf{L^{15}}$ was the one obtained by twisting the π-skeleton of $\mathbf{L^{13}}$. The TPA cross sections of the corresponding complexes $[NBu_4]_3[Eu\mathbf{L^{14}}_3]$ and $[NBu_4]_3[Eu\mathbf{L^{15}}_3]$ decreased to 193 and 96 GM, respectively. However, their luminescence quantum yields increased obviously, with the values of 0.28 and 0.27 for $[NBu_4]_3[Eu\mathbf{L^{14}}_3]$ and $[NBu_4]_3[Eu\mathbf{L^{15}}_3]$, respectively, for which the TPE action cross sections ($\delta \times \Phi_F$) of these two complexes remained in the same level as that of $[NBu_4]_3[Eu\mathbf{L^{13}}_3]$. The stability of complexes $[NBu_4]_3[Eu\mathbf{L^{n}}_3]$ ($n = 13$–15) in water is of prime importance for the further design of bioprobes applicable in biological imaging technique.

Another *in vitro* live cell imaging experiment using an organic–lanthanide complex as the probe was reported in the same year [63]. The tripodal ligand *N*-[2-(bis{2-[(3-methoxybenzoyl)amino]- ethyl}amino)ethyl]-3-methoxybenzamide ($\mathbf{L^{16}}$) was coordinated with $Tb(NO_3)_3$ to form a luminescent complex $[Tb(\mathbf{L^{16}})(NO_3)_3]$, and its multiphoton absorption cross sections were around 3.1 GM for two-photon absorption and 1.9 GM for three-photon absorption. The emission quantum yield was 0.11 in methanol. The authors demonstrated that this Tb^{III} complex can be used as biological probes for the multiphoton imaging of long-term cellular processes with little photodamage. Fig. 15(a)–(c) was the three-photon confocal fluorescent microscopy images (λ_{ex}: 800 nm) of human nasopharyngeal carcinoma (HONE1) cells which were exposed to the Tb^{III} complex in a DMSO–H_2O mixture (DMSO:H_2O = 1:99, 20 μg/mL) for different time. The bright field images of HONE1 cells exposed to the Tb^{III} complex for 24 h (Fig. 15(d)) shows the intact cell membranes of HONE1, indicating the low cytotoxicity of this Tb^{III} probe.

A new complex $Na_2[Eu\mathbf{L^{17}}]$ (Scheme 16) was synthesized by Charbonnière and co-workers [68], in which a coordinating pocket formed by the ligands provided a good shielding of the lanthanide ion from solvent molecules. The number of water molecules in the first coordination sphere of this complex in water and D_2O was close to zero as estimated by the Horrocks' method based on the luminescence lifetimes of the complex [69]. In water, $Na_2[Eu\mathbf{L^{17}}]$ exhibited a typical two-photon absorption behavior upon the excitation at 705 nm, with a TPA cross section of 28.6 GM at 705 nm and a TPE action cross section of 4.3 GM.

The two-photon absorption property of the complex $Eu(tta)_4$·DEASPI (Scheme 10) mentioned in the former section was

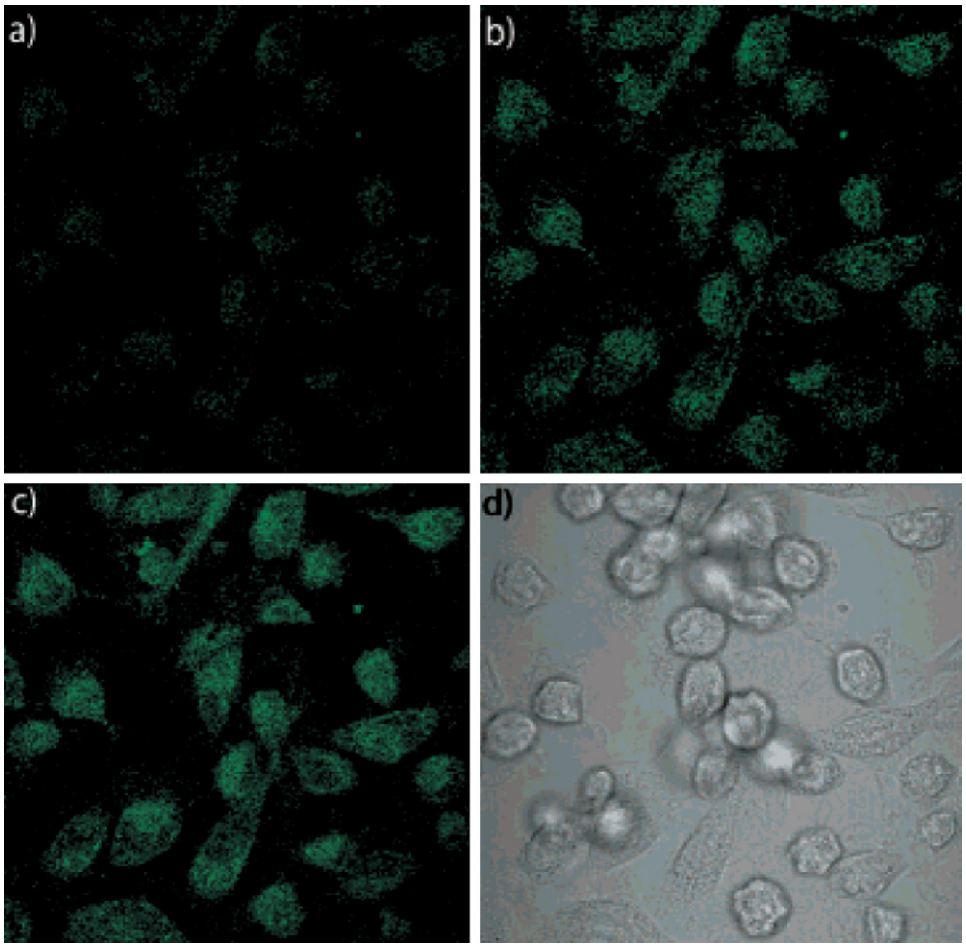

Fig. 15. Three-photon confocal fluorescent microscopy images of HONE1 cells after (a) 3, (b) 45, and (c) 60 min of exposure to the Tb^{III} complex (20 μg/mL in the culture medium, λ_{ex} = 800 nm), showing the Tb^{III} emission above 480 nm. (d) Bright field image of HONE1 cells.
Figure was reproduced from Ref. [63], with permission of the copyright holders.

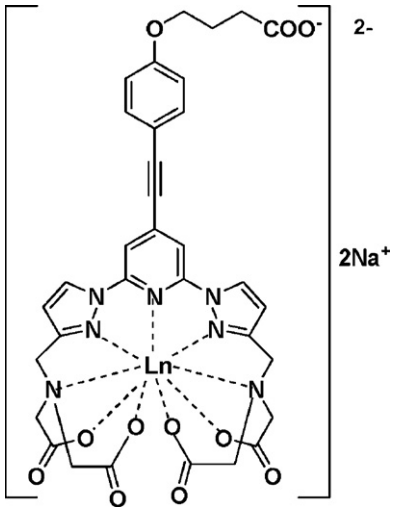

Scheme 16. Structure of the complex $Na_2[EuL^{17}]$.

investigated by Wang and co-workers [37]. The two-photon sensitization wavelength of $Eu(tta)_4$·DEASPI extended beyond 1064 nm and the TPA cross section of this complex was 112 GM at 1064 nm, which was a high value for such a long excitation wavelength. The 1064 nm-ultrafast laser is one of the most frequently used laser sources [70,71], which matches well with the optical window for cells and tissues of 700–1100 nm. Unfortunately, the luminescence quantum yield and TPE action cross section were not provided, so the TPE luminescence efficiency of this complex cannot be estimated.

Very recently, Wong and co-workers reported the two-photon sensitized luminescent properties of an interesting europium complex $Eu(tta)_2Cl$·dpbt (Scheme 17) [72]. $Eu(tta)_2Cl$·dpbt showed a TPA cross section of about 92 GM at 830 nm, and performed target specific to endoplasmic reticulum with advantages of good stability of the sensitization structure in cells, fast uptake, long resident lifetime, low dosage requirement, and low cytotoxicity. Fig. 16 shows the two-photon excitation imaging of $Eu(tta)_2Cl$·dpbt in the endoplasmic reticulum of human cervical carcinoma cells (HeLa).

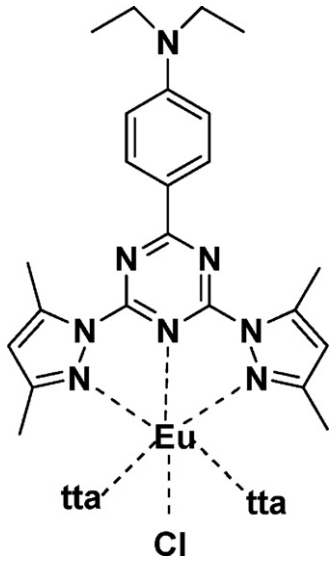

Scheme 17. Structure of complex $Eu(tta)_2Cl$·dpbt.

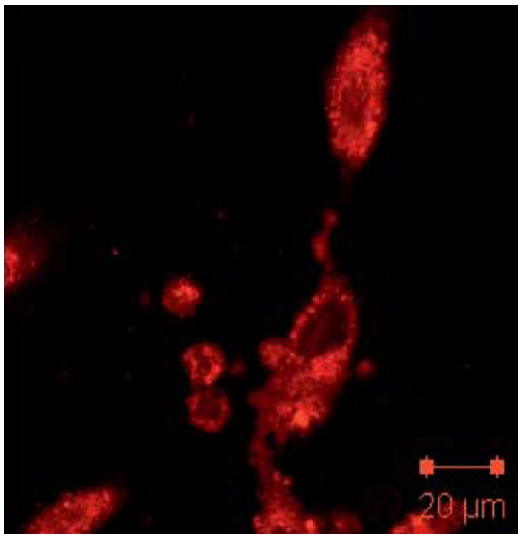

Fig. 16. Two-photon confocal microscopy images of $Eu(tta)_2Cl$·dpbt (λ_{ex} = 800 nm, 1 μg/mL, DMSO:H_2O = 1:99), 30 min exposure in HeLa cells.
Figure was adapted from Ref. [72], with permission of the copyright holders.

4. Nanoparticles based on organic europium complexes

For the application in biosensing or bioimaging, great effort has been focused on the development of novel luminescent Ln^{III} complexes by designing various chromophore ligands. One of the many purposes for this molecular engineering investigation is to meet the demand for luminescent Ln^{III} complexes capable of being efficiently sensitized by long-wavelength light. Another purpose is to increase their solubility and stability in water. However, it is rather a challenge to simultaneously match the demands for good solubility and stability in water solutions of biosamples and efficient long-wavelength sensitization for luminescent lanthanide complexes.

In the past decade, nanoparticles composed of inorganic lanthanide compounds or doped with organic lanthanide complexes have attracted increasing interest for their potential application in fluoroimmunoassay, bioimaging, or other techniques [73]. In comparison with free Ln^{III} complexes, the luminescent nanoparticles possess the additional benefits of remarkable signal amplification and enhanced photostability since each nanoparticle contains a lot of complex molecules shielded by a matrix. However, luminescent nanoparticles of lanthanide complexes which can be efficiently excited by visible-light have so far been scarce.

Recently, we reported the preparation of stable colloidal solutions of $Eu(tta)_3$dpbt nanoparticles in water/methanol mixtures by a precipitation method [74].

The particle size of the prepared $Eu(tta)_3$dpbt nanoparticles could be modulated to some extent by changing the preparation conditions. Fig. 17 shows the TEM images and the size distributions of the $Eu(tta)_3$dpbt nanoparticles with average diameters of 33.1 and 46.7 nm.

Compared with the absorption spectrum of $Eu(tta)_3$dpbt molecules in methanol, the longer-wavelength absorption peaks of the $Eu(tta)_3$dpbt colloidal nanoparticles with average sizes of 33.1 and 46.7 nm red-shifted to 420 nm. The absorption windows of the nanoparticles are much wider than that of $Eu(tta)_3$dpbt in toluene (Fig. 18(a)). The $Eu(tta)_3$dpbt nanoparticles in the colloidal solutions exhibited a wider excitation window for the Eu^{III} luminescence, with the red edge extending up to 475 nm, while $Eu(tta)_3$dpbt in toluene with the same concentration exhibited its excitation window red edge at 441 nm (Fig. 18(b)). The remarkable bathochromic shifts of the absorption and excitation bands of the $Eu(tta)_3$dpbt nanoparticles may originate from the forma-

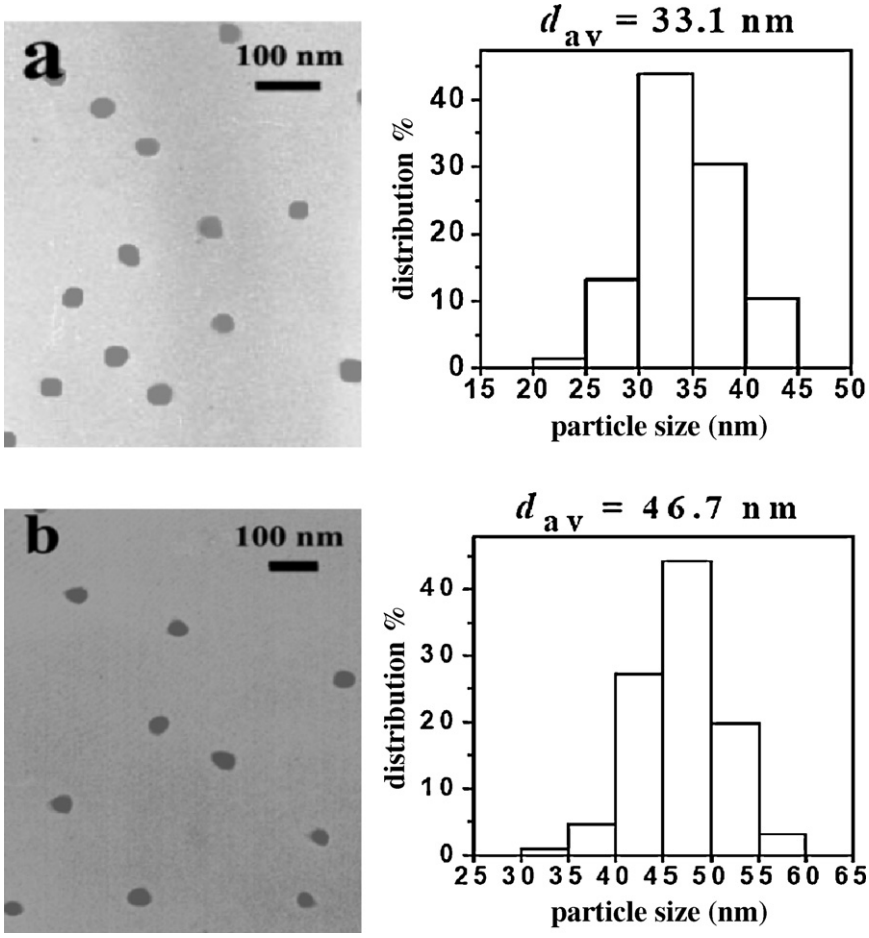

Fig. 17. TEM images of Eu(tta)3dpbt colloidal particles with different sizes.
Figure was reproduced from Ref. [74], with permission of the copyright holders.

tion of J-type aggregates of the polar $Eu(tta)_3$dpbt molecules. This is the first example for significantly expanding the optical excitation window of lanthanide luminescence by forming nanoparticles, which opens an alternative way to match the combined demands for excellent dispersibility in a water solution and high luminescent capability upon long-wavelength optical excitation of lanthanide complexes.

The overall quantum yields for the Eu^{III} emission of $Eu(tta)_3$dpbt in toluene were 0.5 upon the excitation in the wavelength range of 402–430 nm at 10 °C, using 4-dicyanomethylene-2-methyl-6-*p*-dimethylaminostyryl-4H-pyran (DCM) in *n*-propanol (Φ = 0.57) as the reference. However, as listed in Table 3, the quantum yields for the Eu^{III} emission of the $Eu(tta)_3$dpbt colloidal particles were wavelength-dependent, with the values of 0.27, 0.27, 0.24, 0.19, 0.14, and 0.01 upon the excitation at 402, 420, 430, 440, 450, and 475 nm, respectively. This phenomenon can be attributed to the presence of different stacking structures of $Eu(tta)_3$dpbt molecules in nanoparticles which may alter the energetic structures and the processes of excitation energy transfer among ligands and/or to the Eu^{III} luminescent centers.

Table 3
Luminescent capability for $Eu(tta)_3$dpbt molecules as nanoparticles (average diameter, 33.1 nm) and when dissolved in toluene excited at different wavelengths (λ_{ex}). The uncertainty of Φ is 10%.

λ_{ex} (nm)	$\varepsilon\Phi$ ($\times 10^3$ M^{-1} cm^{-1})	
	$Eu(tta)_3$dpbt nanoparticle	$Eu(tta)_3$dpbt molecules in toluene
402	9.8	37.8
420	11.8	9.1
430	9.9	2.4
440	6.5	n.d.
450	3.4	n.d.
475	0.1	n.d.

For the colloidal particles, the photoluminescence decay kinetics at the probing wavelength of 616 nm, corresponding to the $^5D_0 \rightarrow {}^7F_2$ transition of $Eu(tta)_3$dpbt, could be well accounted for by a three-exponential decay model function, which yielded the apparent decay time constants of 416, 221, and 69 μs. The longest (416 μs) is close to the decay time of the free $Eu(tta)_3$dpbt molecules in toluene (480 μs), and it is likely that the additional shorter-lived components should be partially responsible for the relatively low luminescence quantum yield with respect to $Eu(tta)_3$dpbt molecules in the toluene solution.

Because the excitation window red edge of the $Eu(tta)_3$dpbt nanoparticles bathochromically shifted relative to that of $Eu(tta)_3$dpbt molecules in toluene, $Eu(tta)_3$dpbt molecules in the nanoparticles showed obviously enhanced luminescent capability ($\varepsilon \times \Phi$) upon the excitation at long wavelengths (λ_{ex} > 420 nm) compared to that dissolved in toluene as can be seen in Table 3.

The $Eu(tta)_3$dpbt nanoparticles exhibited excellent two-photon sensitized luminescent properties, with a TPE band locating at 832 nm (Fig. 19), red-shifting by 24 nm compared to that of $Eu(tta)_3$dpbt molecules dissolved in toluene. From the density of a solid sample of $Eu(tta)_3$dpbt, it can be estimated that a $Eu(tta)_3$dpbt nanoparticle (d_{av} = 33.1 nm) contains about 8.5×10^3 $Eu(tta)_3$dpbt

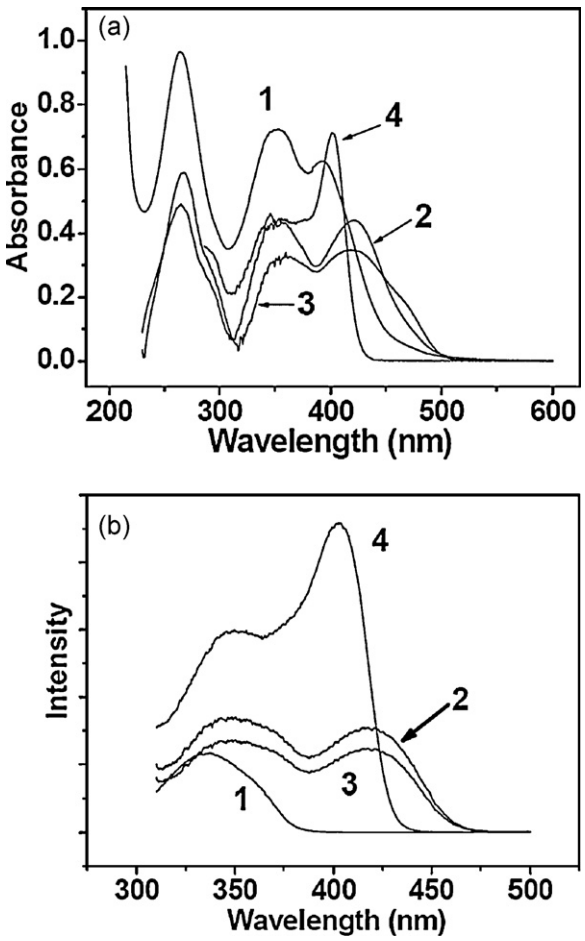

Fig. 18. (a) UV–vis absorption spectra and (b) fluorescence excitation spectra (λ_{em} = 614 nm). (1) Eu(tta)3dpbt in methanol; (2) colloidal solution of Eu(tta)3dpbt nanoparticles with d_{av} = 33.1 nm; (3) colloidal solution of Eu(tta)$_3$dpbt nanoparticles with d_{av} = 46.7 nm; (4) Eu(tta)$_3$dpbt free in toluene. The Eu(tta)$_3$dpbt concentration in all of these samples was 1×10^{-5} mol L^{-1}.
Figure was adapted from Ref. [74], with permission of the copyright holders.

molecules. This estimation yields the maximum TPA action cross section of the Eu(tta)$_3$dpbt nanoparticles (d_{av} = 33.1 nm) of 3.2×10^5 GM, which is about seven times higher than the highest value reported for the CdSe/ZnS core-shell quantum dots [75].

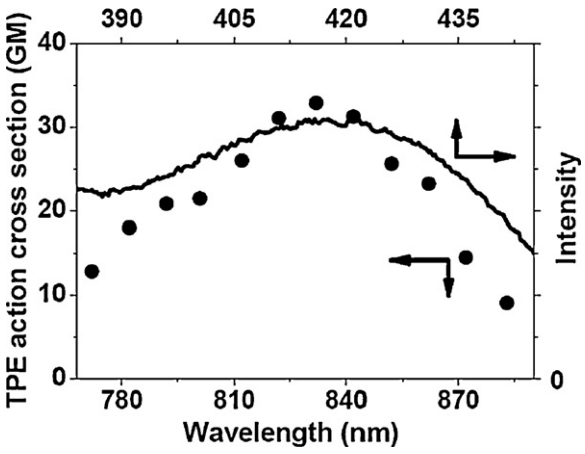

Fig. 19. Two-photon excitation action cross sections ($\delta\ \Phi$) (●) and one-photon excitation spectrum (λ_{em} = 614 nm) (solid line) for the Eu(tta)$_3$dpbt nanoparticles. The experimental uncertainty for the two-photon excitation action cross sections is about 15%.
Figure was reproduced from Ref. [74], with permission of the copyright holders.

The favorable luminescent properties and the good dispersibility in water–methanol solutions of the Eu(tta)$_3$dpbt nanoparticles are very promising for the development of new luminescent nanoprobes for bioanalysis.

The excellent long-wavelength sensitized luminescent properties of Eu(tta)$_3$dpbt and its derivatives has stimulated the efforts to develop bionanoprobes, in which the Eu^{III} ion sensitized by chromophores such as dpbt are embed in a matrix of nanoscopic particles. These efforts aimed at endowing the synthesized nanoprobes with anticipant luminescence properties, especially the Eu^{III} luminescence efficiently sensitized by visible-light or TPA of NIR light, high brightness, high photostability, excellent dispersibility in water solutions and bio-compatibility. The delay of the emergence of satisfactory examples for such nanoprobes is due to the difficult in encapsulating these long-wavelength sensitized luminescent europium complexes in suitable water-dispersible nanoparticles without total or partial loss of the intrinsic luminescent properties of the complexes. The simple use of Eu(tta)$_3$dpbt in the preparation of luminescent nanoparticles with conventional microemulsion polymerization [76] or Stöber method [77] seems impossible to maintain its luminescent properties because of the reactions between the complexes with compounds appearing in the these processes as demonstrated by the experimental results of our group and other groups. Recently, we have succeed in developing new processes for the encapsulation of Eu(tta)$_3$dpbt and its derivatives to prepare bionanoprobes with desirable luminescent properties which will be reported elsewhere.

An alternative method for the encapsulation of dpbt-sensitized Eu^{III} complexes in water-dispersible nanoparticles was proposed by Yuan and co-workers [73d]. An APS-CDHH-Eu^{III}-DPBT complex (Scheme 18(a)) was synthesized and used as a precursor in the hydrolysis copolymerization with free 3-aminopropyl(triethoxyl)silane (APS) and tetraethyl orthosilicate (TEOS) in a water-in-oil (W/O) microemulsion system composed of dioctyl sulfosuccinate (AOT), heptane, toluene and water to produce silica-based luminescence nanoparticles with average diameter of 10 nm. The aromatic bridge between β-diketonate and

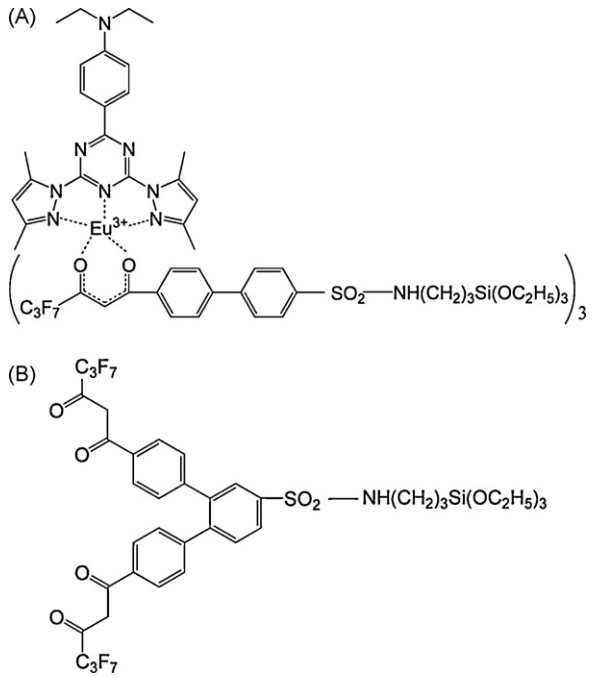

Scheme 18. Possible structures of Eu(CDHH-APS)$_3$DPBT (a) and BHHCT-APS ligand (b).

APS fragments played a role in reducing the attack on APS-CDHH-Eu^{III}-DPBT from other chemicals during the encapsulation process. By the sensitization effect of dpbt, APS-CDHH-Eu^{III}-DPBT exhibited an excitation band centered at 406 nm for the Eu^{III} luminance; however, the excitation spectrum of the produced nanoparticles showed a shoulder band at 384 nm with an edge extending up to 450 nm, implying the partial lose of the long-wavelength sensitized luminescent properties of APS-CDHH-Eu^{III}-DPBT in the copolymerization process.

More recently, this procedure for the preparation of visible-light-sensitized luminescent nanoprobe was improved by replacing CDHH in APS-CDHH-Eu^{III}-DPBT with BHHCT (Scheme 18(b)) to from a new precursor APS-BHHCT-Eu^{III}-DPBT and changing the reverse microemulsion to a system composed of Triton X-100, n-octanol, cyclohexane and water [73e]. APS-BHHCT-Eu^{III}-DPBT exhibited luminescence excitation bands centered at 406 and 335 nm, while the intensity ratio of the band at visible-light region to that at UV region is much lower than that of APS-CDHH-Eu^{III}-DPBT. The UV–vis absorption spectrum of the prepared nanoparticles in 0.05 M Tris–HCl buffer, with an average diameter of 36 nm and narrow size distribution, exhibited strong scattering in the visible-light region (over 500 nm) and a small absorption band centered at about 425 nm which might be related to molecular aggregates of Eu^{III} complexes containing dpbt. Due to the strong scattering background of the absorption spectrum of the nanoparticles, the quantum yield of Eu^{III} luminescence of these nanoparticles is not high because most photons reaching the particles were scattered away, although the dpbt-sensitized Eu^{III} complexes in the nanoparticles are efficient visible-light-sensitized luminescence dyes. Nanoprobes formed by labeling streptavidin (SA) with these visible-light-sensitized nanoparticles were successfully used for time-gated luminescence imaging of *Giardia lamblia* in a concentrated environmental water sample, showing promising prospect for living cell imaging based on nanoprobes encapsulating long-wavelength sensitized europium complexes.

5. Conclusion

Remarkable progress has been achieved in the design and synthesis of long-wavelength sensitized luminescent europium complexes in the last two decades. Europium complexes sensitized by dpbt and other excellent antenna ligands are promising building blocks for the development of bioprobes with the advantages of high sensitivity, specific targeting imaging ability, deep penetration and less damage to the biosamples. Increased effort should be paid to face the great challenges in the related fields. These include a better understanding of the detailed mechanism of the singlet energy-transfer pathway in luminescent europium complexes, the need to create new chromophore ligands with efficient visible-light-sensitized and two-photon-sensitized capability for the luminescence of Eu^{III}, Nd^{III}, Er^{III} or Yb^{III} ion, designing and synthesizing water soluble lanthanide complexes emitting visible and NIR light upon long-wavelength sensitization, developing novel approaches for the encapsulation of the long-wavelength sensitized lanthanide complexes in small nanoparticles that are capable of being well dispersed in water solutions and linked with biomolecules for detection.

Acknowledgment

The authors express their thanks for the joint support by NSFC (Project Nos. 50821061, 90606017, 20973003), NKBRSF (G2006CB806102) and 863 program (2006AA02090405) from the Chinese Ministry of Science and Technology.

References

[1] W.T. Carnall, in: K.A. Gschneidner Jr., L. Eyring (Eds.), Handbook on the Physics and Chemistry of Rare Earths, vol. 3, North Holland Publ. Co., Amsterdam, 1979, p. 172.
[2] J.-C.G. Bünzli, S. Comby, A.S. Chauvin, C.D.B. Vandevyver, J. Rare Earths 25 (2007) 257.
[3] (a) J.-C.G. Bünzli, C. Piguet, Chem. Soc. Rev. 34 (2005) 1048;
(b) S.V. Eliseeva, J.-C.G. Bünzli, Chem. Soc. Rev. 39 (2010) 189;
(c) J.-C.G. Bünzli, S.V. Eliseeva, in: P. Hänninen, H. Härmä (Eds.), Springer Series on Fluorescence, vol. 7. Lanthanide Spectroscopy, Materials, and Bio-applications, Springer Verlag, Berlin, 2010 (Chapter 2).
[4] W.T. Carnall, P.R. Fields, K. Rajnak, J. Chem. Phys. 49 (1968) 4424.
[5] W.T. Carnall, P.R. Fields, K. Rajnak, J. Chem. Phys. 49 (1968) 4443.
[6] W.T. Carnall, P.R. Fields, K. Rajnak, J. Chem. Phys. 49 (1968) 4447.
[7] W.T. Carnall, P.R. Fields, K. Rajnak, J. Chem. Phys. 49 (1968) 4450.
[8] M.H.V. Werts, R.T.F. Jukes, J.W. Verhoeven, Phys. Chem. Chem. Phys. 4 (2002) 1542.
[9] (a) S. Sato, M. Wada, Bull. Chem. Soc. Jpn. 43 (1970) 1955;
(b) D. Parker, J.A.G. Williams, J. Chem. Soc., Dalton Trans. (1996) 3613;
(c) M. Latva, H. Takalo, V.M. Mukkala, C. Matachescu, J.C. Rodríguez-Ubis, J. Kankare, J. Lumin. 75 (1997) 149;
(d) R.D. Archer, H.Y. Chen, L.C. Thompson, Inorg. Chem. 37 (1998) 2089;
(e) A. Dadabhoy, S. Faulkner, P.G. Sammes, J. Chem. Soc., Perkin Trans. 2 (2002) 348;
(f) F. Gutierrez, C. Tedeschi, L. Maron, J.P. Daudey, R. Poteau, J. Azema, P. Tisnes, C. Picard, Dalton Trans. (2004) 1334.
[10] F.J. Steemers, W. Verboom, D.N. Reinhoudt, E.B. van der Tol, J.W. Verhoeven, J. Am. Chem. Soc. 117 (1995) 9408.
[11] M.J. Levene, D.A. Dombeck, K.A. Kasische, R.P. Molloy, W.W. Webb, J. Neurophysiol. 91 (2004) 1908.
[12] H.L. Handl, J. Vagner, H.I. Yamamura, V.J. Hruby, R.J. Gillies, Anal. Biochem. 330 (2004) 242.
[13] M. Santos, B.C. Roy, H. Goicoechea, A.D. Campiglia, S. Mallik, J. Am. Chem. Soc. 126 (2004) 10738.
[14] T. Terai, K. Kikuchi, S.Y. Iwasawa, T. Kawabe, Y. Hirata, Y. Urano, T. Nagano, J. Am. Chem. Soc. 128 (2006) 6938.
[15] R.F. Ziessel, G. Ulrich, L. Charbonnière, D. Imbert, R. Scopelliti, J.C.G. Bünzli, Chem. Eur. J. 12 (2006) 5060.
[16] R. Weissleder, V. Ntziachristos, Nat. Med. 9 (2003) 123.
[17] M.H.V. Werts, M.A. Duin, J.W. Hofstraat, J.W. Verhoeven, Chem. Commun. (1999) 799.
[18] A. Dadabhoy, S. Faulkner, P.G. Sammes, J. Chem. Soc., Perkin Trans. 2 (2000) 2359.
[19] A. Beeby, L.M. Bushby, D. Maffeo, J.A.G. Williams, J. Chem. Soc., Perkin Trans. 2 (2000) 1281.
[20] Y. Bretonniere, M.J. Cann, D. Parker, R. Slater, Chem. Commun. (2002) 1930.
[21] S.I. Klink, L. Grave, D.N. Reinhoudt, F.C.J.M. van Veggel, M.H.F. Werts, F.A.J. Geurts, J.W. Hofstraat, J. Phys. Chem. A 104 (2000) 5457.
[22] J.B. Oh, Y.H. Kim, M.K. Nah, H.K. Kim, J. Lumin. 111 (2005) 255.
[23] G.A. Crosby, Mol. Cryst. 1 (1966) 37.
[24] W.D. Horrocks Jr., W.E. Collier, J. Am. Chem. Soc. 103 (1981) 2856.
[25] J. Bruno, W.D. Horrocks Jr., R.J. Zauhar, Biochemistry 31 (1992) 7016.
[26] S.I. Klink, G.A. Hebbink, L. Grave, P.G.B. Oude Alink, F.C.J.M. van Veggel, M.H.V. Werts, J. Phys. Chem. A 106 (2002) 3681.
[27] G.F. de Sá, O.L. Malta, C. de Mello Donegá, A.M. Simas, R.L. Longo, P.A. Santa-Cruz, E.F. da Silva Jr., Coord. Chem. Rev. 196 (2000) 165.
[28] C. Yang, L.M. Fu, Y. Wang, J.P. Zhang, W.T. Wong, X.C. Ai, Y.F. Qiao, B.S. Zou, L.L. Gui, Angew. Chem. Int. Ed. 43 (2004) 5010.
[29] K.A. Gschneider Jr., L. Eyring, Handbook on the Physics and Chemistry of Rare Earths, vol. 3, North-Holland, Amsterdam, 1979.
[30] V. Vicinelli, P. Ceroni, M. Maestri, V. Balzani, M. Gorka, F. Vögtle, J. Am. Chem. Soc. 124 (2002) 6461.
[31] J.-C.G. Bunzli, E. Moret, V. Foiret, K.J. Schenk, W. Mingzhao, J. Linpei, J. Alloys Compd. 207 (1994) 107.
[32] R. Van Deun, P. Nockemann, P. Fias, K. Van Hecke, L. Van Meervelt, K. Binnemans, Chem. Commun. (2005) 590.
[33] R. Hao, M.Y. Li, Y. Wang, J.P. Zhang, Y. Ma, L.M. Fu, X.F. Wen, Y.S. Wu, X.C. Ai, S.W. Zhang, Y.G. Wei, Adv. Funct. Mater. 17 (2007) 3663.
[34] (a) S.M. Borisov, O.S. Wolfbeis, Anal. Chem. 78 (2006) 5094;
(b) M.E. Koese, B.F. Carrol, K.S. Schanze, Langmuir 21 (2005) 9121;
(c) S.M. Borisov, G.S. Vasylevska, C. Krause, O.S. Wolfbeis, Adv. Funct. Mater. 16 (2006) 1536.
[35] F. Xue, Y. Ma, L. Fu, R. Hao, G. Shao, M. Tang, J. Zhang, Y. Wang, Phys. Chem. Chem. Phys. (2010), doi:10.1039/b920448b.
[36] P. Kadjane, L. Charbonnière, F. Camerel, P.P. Lainé, R. Ziessel, J. Fluoresc. 18 (2008) 119.
[37] M. Shi, C. Ding, J. Dong, H. Wang, Y. Tian, Z. Hu, Phys. Chem. Chem. Phys. 11 (2009) 5119.
[38] N.M. Shavaleev, S.J.A. Pope, Z.R. Bell, S. Faulkner, M.D. Ward, Dalton Trans. (2003) 808.
[39] G.A. Hebbink, S.I. Klink, L. Grave, P.G.B. Oude Alink, F.C.J.M. van Veggel, ChemPhysChem 3 (2002) 1014.
[40] J.R.G. Thoren, J.M. Rey, R.G. Denning, S.E. Watkins, M. Etchells, M. Green, V. Christou, J. Phys. Chem. A 106 (2002) 4014.

[41] N.S. Baek, Y.H. Kim, S.G. Roh, B.K. Kwak, H.K. Kim, Adv. Funct. Mater. 16 (2006) 1873.
[42] G. Mancino, A.J. Ferguson, A. Beeby, N.J. Long, T.S. Jones, J. Am. Chem. Soc. 127 (2005) 524.
[43] G.S. He, L.-S. Tan, Q. Zheng, P.N. Prasad, Chem. Rev. 108 (2008) 1245.
[44] (a) B.H. Cumpston, S.P. Ananthavel, S. Barlow, D.L. Dyer, J.E. Ehrlich, L.L. Erskine, A.A. Heikal, S.M. Kuebler, I.Y. Sandy-Lee, D. McCord-Maughon, J. Qin, H. Röckel, M. Rumi, X.L. Wu, S.R. Marder, J.R. Perry, Nature 398 (1999) 51;
(b) D. Dini, M.J.F. Calvete, M. Hanack, V. Amendola, M. Meneghetti, Chem. Commun. (2006) 2394.
[45] K.D. Belfield, X. Ren, E.W. Van Stryland, D.J. Hagan, V. Dubikovsky, E.J. Miesak, J. Am. Chem. Soc. 122 (2000) 1217.
[46] (a) W.R. Zipfel, R.M. Williams, W.W. Webb, Nat. Biotechnol. 21 (2003) 1369;
(b) M.A. Oar, J.M. Serin, W.R. Dichtel, J.M.J. Fréchet, T.Y. Ohulchanskyy, P.N. Prasad, Chem. Mater. 17 (2005) 2267.
[47] (a) F. Bestvater, E. Spiess, G. Stobrawa, M. Hacker, T. Feurer, T. Porwol, U. Berchner-Pfannschmidt, C. Wotzlaw, H.J. Acker, Microscope (Oxford, U.K.) 208 (2002) 108;
(b) P. Schwille, Cell Biochem. Biophys. 34 (2001) 383.
[48] L.M. Fu, X.F. Wen, X.C. Ai, Y. Sun, Y.S. Wu, J.P. Zhang, Y. Wang, Angew. Chem. Int. Ed. 44 (2005) 747.
[49] G.F. White, K.L. Litvinenko, S.R. Meech, D.L. Andrews, A.J. Thomson, Photochem. Photobiol. Sci. 3 (2004) 47.
[50] A. Picot, F. Malvolti, B.L. Guennic, P.L. Baldeck, J.A.G. Williams, C. Andraud, O. Maury, Inorg. Chem. 46 (2007) 2659.
[51] G. Piszczek, B.P. Malinal, I. Gryczynski, J. Dattelbaum, J.R. Lakowicz, J. Fluoresc. 11 (2001) 101.
[52] G. Piszczek, I. Gryczynski, B.P. Malinal, J.R. Lakowicz, J. Fluoresc. 12 (2002) 15.
[53] K.L. Wong, G.L. Law, W.M. Kwok, W.T. Wong, D.L. Phillips, Angew. Chem. Int. Ed. 44 (2005) 3436.
[54] M.H.V. Werts, N. Nerambourg, D. Pélégry, Y.L. Grand, M. Blanchard-Desce, Photochem. Photobiol. Sci. 4 (2005) 531.
[55] W. Kaiser, C.G.B. Garrett, Phys. Rev. Lett. 7 (1961) 229.
[56] J.R. Lakowicz, G. Piszczek, B.P. Maliwal, I. Gryczynski, ChemPhysChem 4 (2001) 247.
[57] C. Xu, W. Zipfel, J.B. Shear, R.M. Williams, W.W. Webb, Proc. Natl. Acad. Sci. U.S.A. 93 (1996) 10763.
[58] (a) M. Albota, D. Beljonne, J.L. Brédas, J.E. Ehrlich, J.Y. Fu, A.A. Heikal, S.E. Hess, T. Kogej, M.D. Levin, S.R. Marder, D. McCord-Maughon, J.W. Perry, H. Röckel, M. Rumi, G. Subramaniam, W.W. Webb, X.L. Wu, C. Xu, Science 281 (1998) 1653;
(b) L. Ventelon, S. Charier, L. Moreaux, J. Mertz, M. Blanchard-Desce, Angew. Chem. Int. Ed. 113 (2001) 2156;
(c) L. Ventelon, S. Charier, L. Moreaux, J. Mertz, M. Blanchard-Desce, Angew. Chem. Int. Ed. 40 (2001) 2098;
(d) B. Dick, G. Hohlneicher, J. Chem. Phys. 76 (1982) 5755;
(e) B.A. Reinhardt, L.L. Brott, S.J. Clarson, A.G. Dillard, J.C. Bhatt, R. Kannan, Chem. Mater. 10 (1998) 1863;
(f) J. Zimmermann, P.A. Linden, H.M. Vaswani, R.G. Hiller, G.R. Fleming, J. Phys. Chem. B 106 (2002) 9418.
[59] (a) J.E. Rogers, J.E. Slagle, D.G. McLean, R.L. Sutherland, B. Sankaran, R. Kannan, L.S. Tan, P.A. Fleitz, J. Phys. Chem. A 108 (2004) 5514;
(b) B.R. Cho, K.H. Son, S.H. Lee, Y.S. Song, Y.K. Lee, S.J. Jeon, J.H. Choi, H. Lee, M. Cho, J. Am. Chem. Soc. 123 (2001) 10039.
[60] (a) S. Abe, Chem. Phys. 264 (2001) 355;
(b) C.K. Wang, P. Macak, Y. Luo, H. Ågren, J. Chem. Phys. 114 (2001) 9813;
(c) D. Beljonne, W. Wenseleers, E. Zojer, Z. Shuai, H. Vogel, S.J.K. Pond, J.W. Perry, S.R. Marder, J.L. Brédas, Adv. Funct. Mater. 12 (2002) 631.
[61] F.C. Grozema, R. Telesca, H.T. Jonkman, L.D.A. Siebbeles, J.G. Snijders, J. Chem. Phys. 115 (2001) 10014.
[62] A. Picot, A. D'Aléo, P.L. Baldeck, A. Grichine, A. Duperray, C. Andraud, O. Maury, J. Am. Chem. Soc. 130 (2008) 1532.
[63] G.L. Law, K.L. Wong, C.W.Y. Man, W.T. Wong, S.W. Tsao, M.H.W. Lam, P.K.S. Lam, J. Am. Chem. Soc. 130 (2008) 3714.
[64] A.D. Aléo, A. Picot, P.L. Baldeck, C. Andraud, O. Maury, Inorg. Chem. 47 (2008) 10269.
[65] A.E. Martell, R.M. Smith, Values from Critical Stability Constant, Plenum Press, New York, 1974.
[66] (a) J.J. Lessmann, W.D. Horrocks Jr., Inorg. Chem. 39 (2000) 3114;
(b) N. Ouali, B. Bocquet, S. Rigault, P.Y. Morgantini, J. Weber, C. Piguet, Inorg. Chem. 41 (2002) 1436;
(c) A.S. Chauvin, F. Gumy, D. Imbert, J.C.G. Bünzli, Spectros. Lett. 37 (2004) 517.
[67] A. Hayek, F. Bolze, J.F. Nicoud, P.L. Baldeck, Y. Mély, Photochem. Photobiol. Sci. 5 (2006) 102.
[68] P. Kadjane, M. Starck, F. Camerel, D. Hill, N. Hildebrandt, R. Ziessel, L.J. Charbonnière, Inorg. Chem. 48 (2009) 4601.
[69] (a) A. Beeby, I.M. Clarkson, R.S. Dickins, S. Faulkner, D. Parker, L. Royle, A.S. de Sousa, J.A.G. Williams, M. Woods, J. Chem. Soc., Perkin Trans. 2 (1999) 493;
(b) R.M. Supkowski, W.D.W. Horrocks Jr., Inorg. Chim. Acta 340 (2002) 44.
[70] A. Jenei, A.K. Kirsch, V. Subramaniam, D.J. Arndt-Jovin, T.M. Jovin, Biophys. J. 76 (1999) 1092.
[71] T.L. Wee, Y.K. Tzeng, C.C. Han, H.C. Chang, W.S. Fann, J.H. Hsu, K.M. Chen, Y.C. Yu, J. Phys. Chem. A 111 (2007) 9379.
[72] G.L. Law, K.L. Wong, C.W.Y. Man, S.W. Tsao, W.T. Wong, J. Biophoton. 2 (2009) 718.
[73] (a) X.D. Hai, M.Q. Tan, G.L. Wang, Z.Q. Ye, J.L. Yuan, K. Matsumoto, Anal. Sci. 20 (2004) 245;
(b) R. Si, Y.W. Zhang, L.P. You, C.H. Yan, Angew. Chem., Int. Ed. 44 (2005) 3256;
(c) H.S. Peng, C.F. Wu, Y.F. Jiang, S.H. Huang, J. McNeill, Langmuir 23 (2007) 1591;
(d) J. Wu, G.L. Wang, D.Y. Jin, J.L. Yuan, Y.F. Guan, J. Piper, Chem. Commum. (2008) 365;
(e) J. Wu, Z.Q. Ye, G.L. Wang, D.Y. Jin, J.L. Yuan, Y.F. Guan, J. Piper, J. Mater. Chem. 19 (2009) 1258.
[74] X.F. Wen, M.Y. Li, Y. Wang, J.P. Zhang, L.M. Fu, R. Hao, Y. Ma, X.C. Ai, Langmuir 24 (2008) 6932.
[75] (a) D.R. Larson, W.R. Zipfel, R.M. Williams, S.W. Clark, M.P. Bruchez, F.W. Wise, W.W. Webb, Science 300 (2003) 1434;
(b) A. Komoto, S. Maenosono, Y. Yamaguchi, Physica E 24 (2004) 74.
[76] F.J. Arriagad, K. Osseo-Asare, J. Colloid Interface Sci. 170 (1995) 8.
[77] W. Stöber, A. Fink, E. Bohn, J. Colloid Interface Sci. 26 (1968) 62.